

R. Ludwig and G. Bogdanov
“RF Circuit Design: Theory and Applications”
2nd edition

Figures for Chapter 8

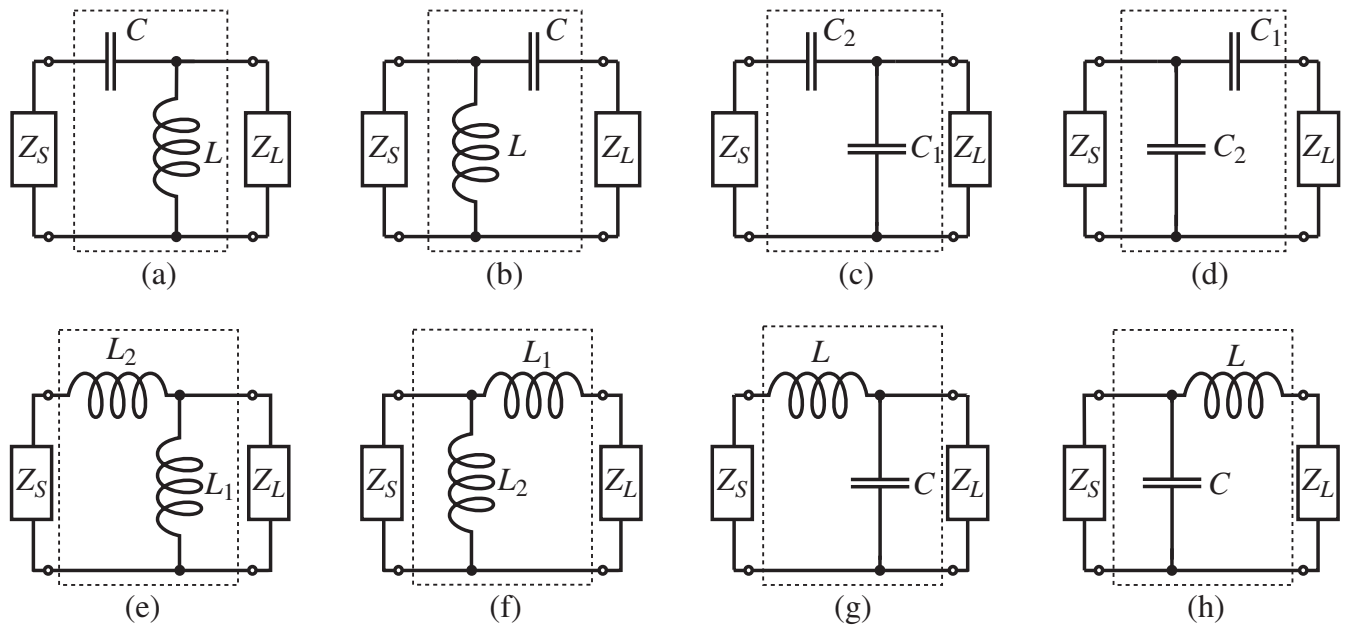


Figure 8-1 Eight possible configurations of discrete two-component matching networks.

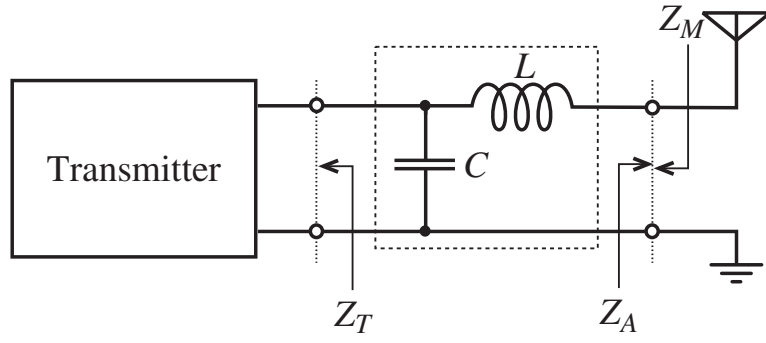


Figure 8-2 Transmitter to antenna matching circuit design.

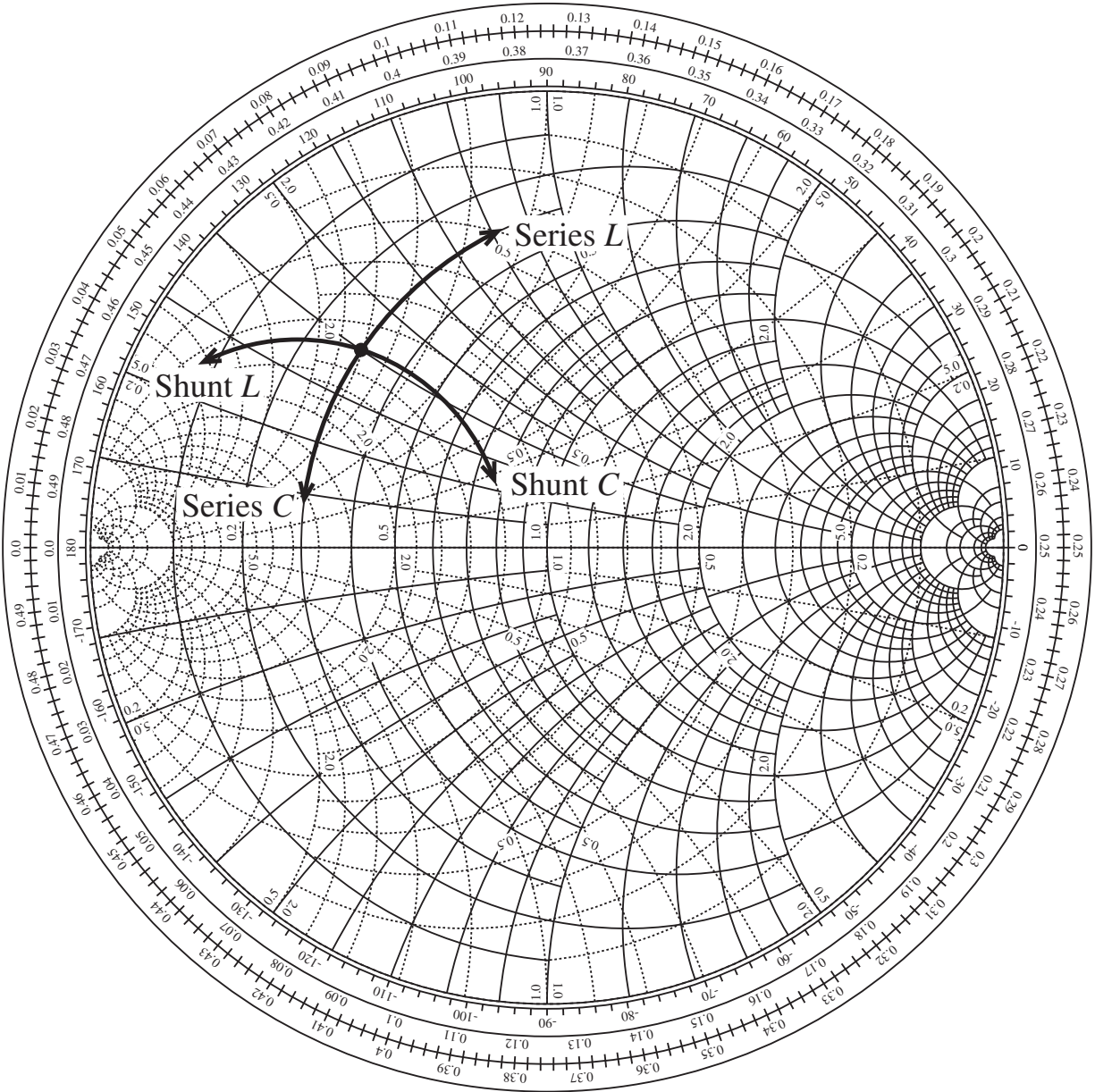


Figure 8-3 Impedance effect of series and shunt connections of L and C to a complex load in the Smith Chart.

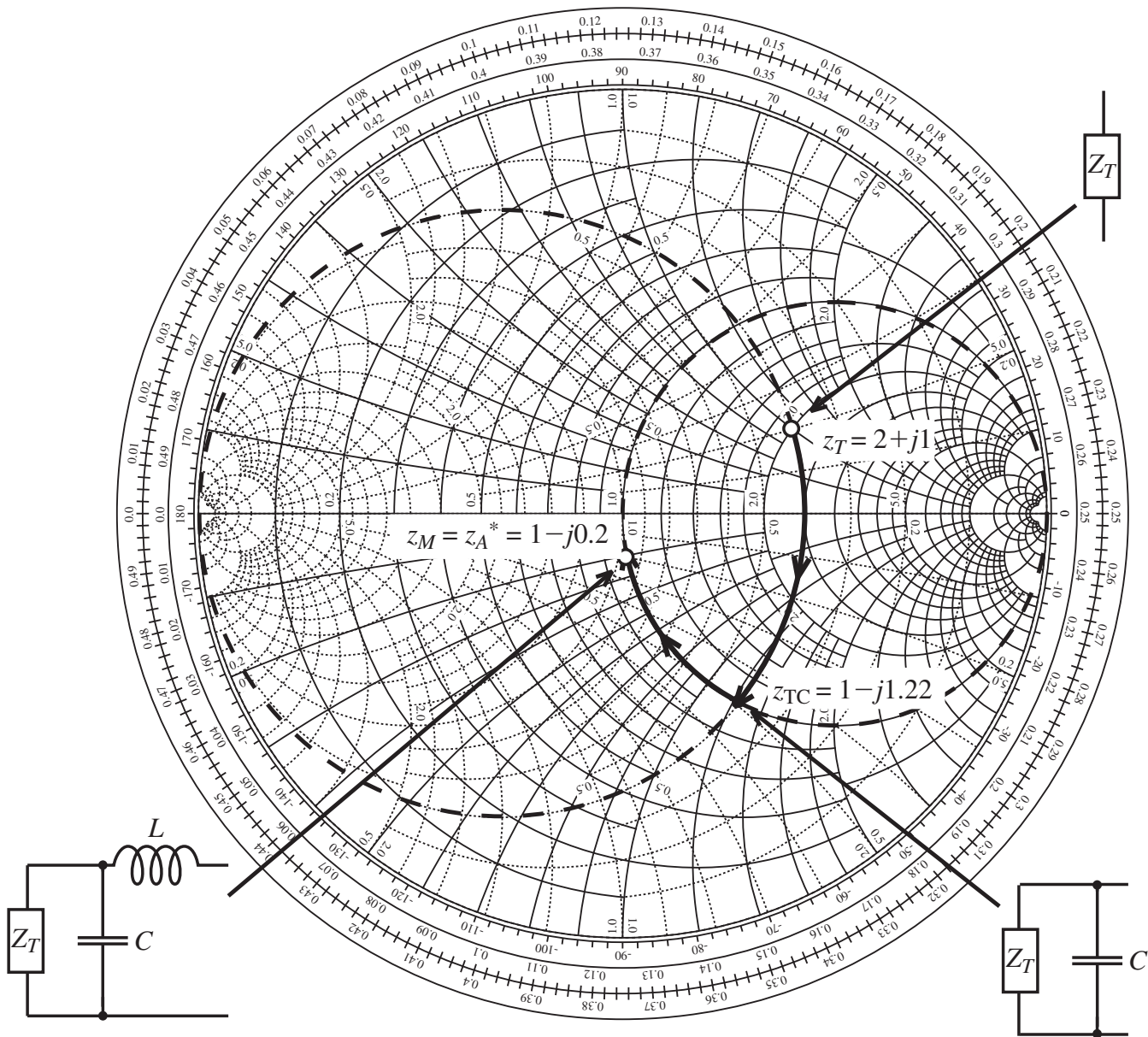


Figure 8-4 Design of the two-element matching network as part of the ZY Smith Chart.

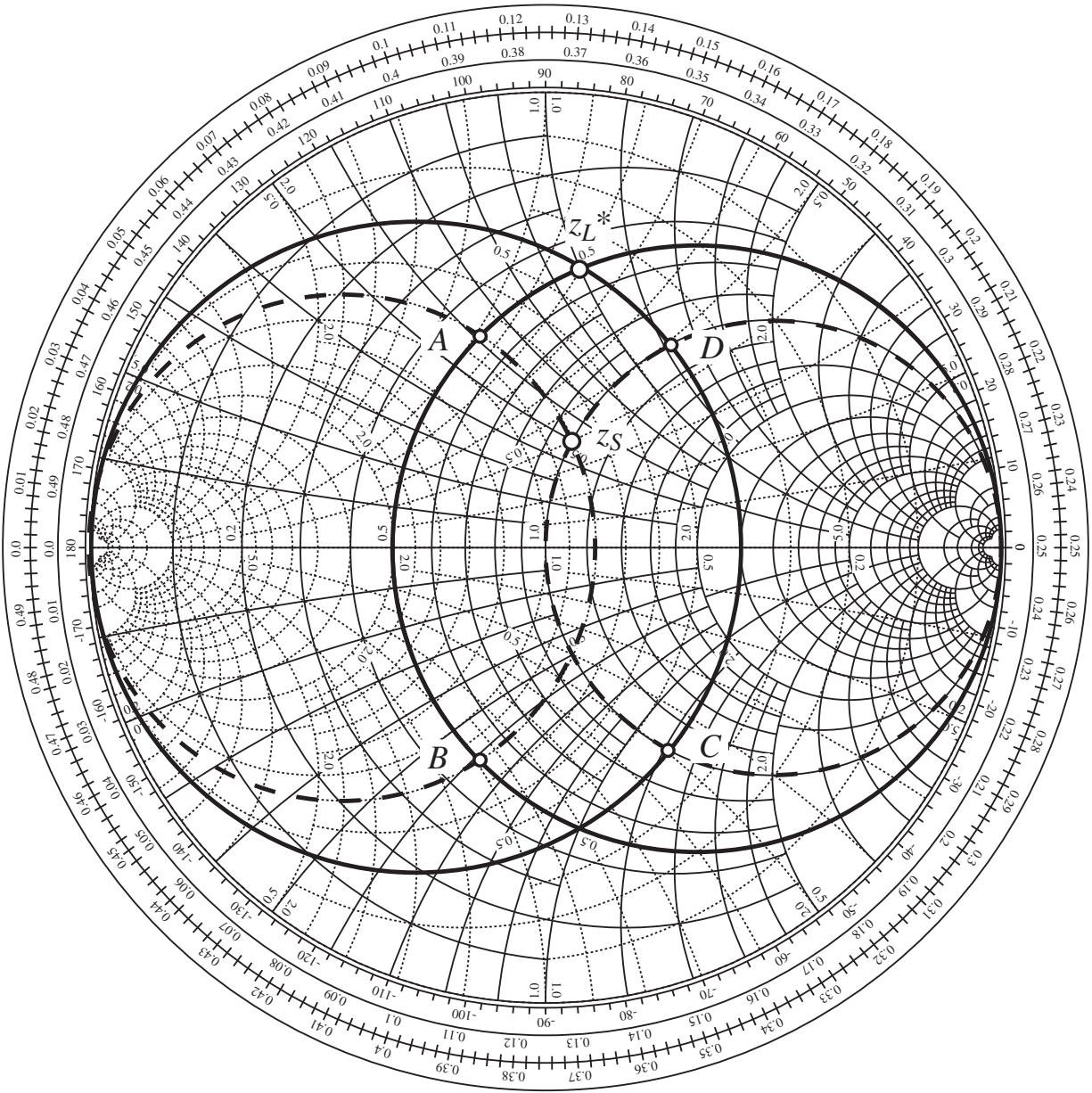


Figure 8-5 Design of a matching network using the Smith Chart

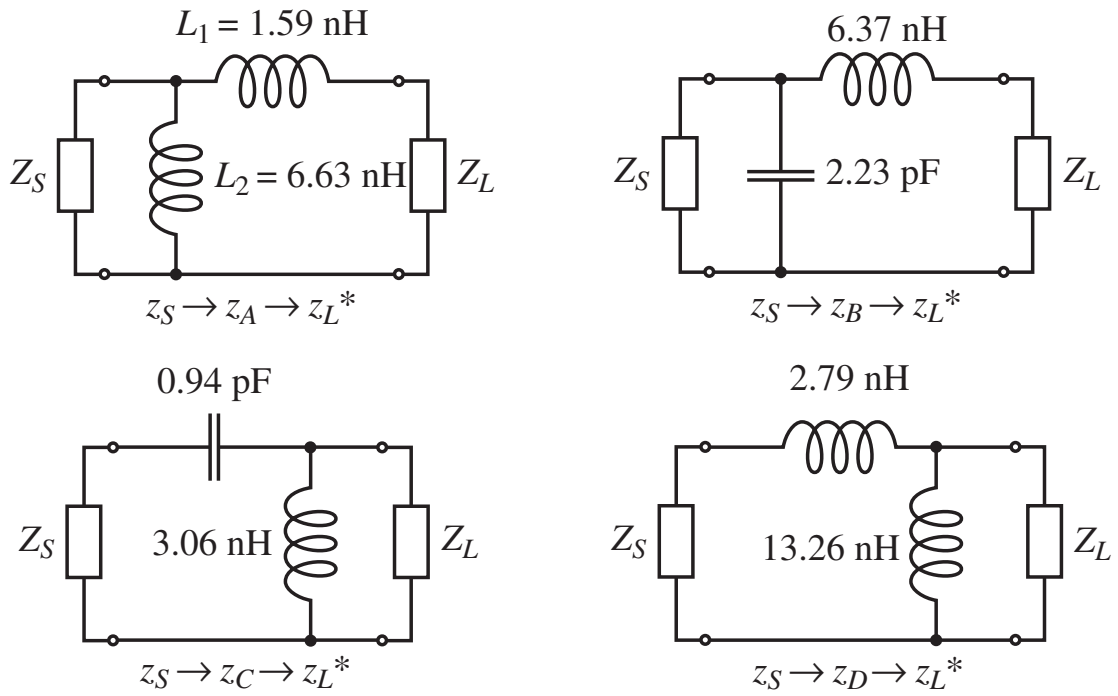


Figure 8-6 Matching networks for four different paths in the Smith Chart.

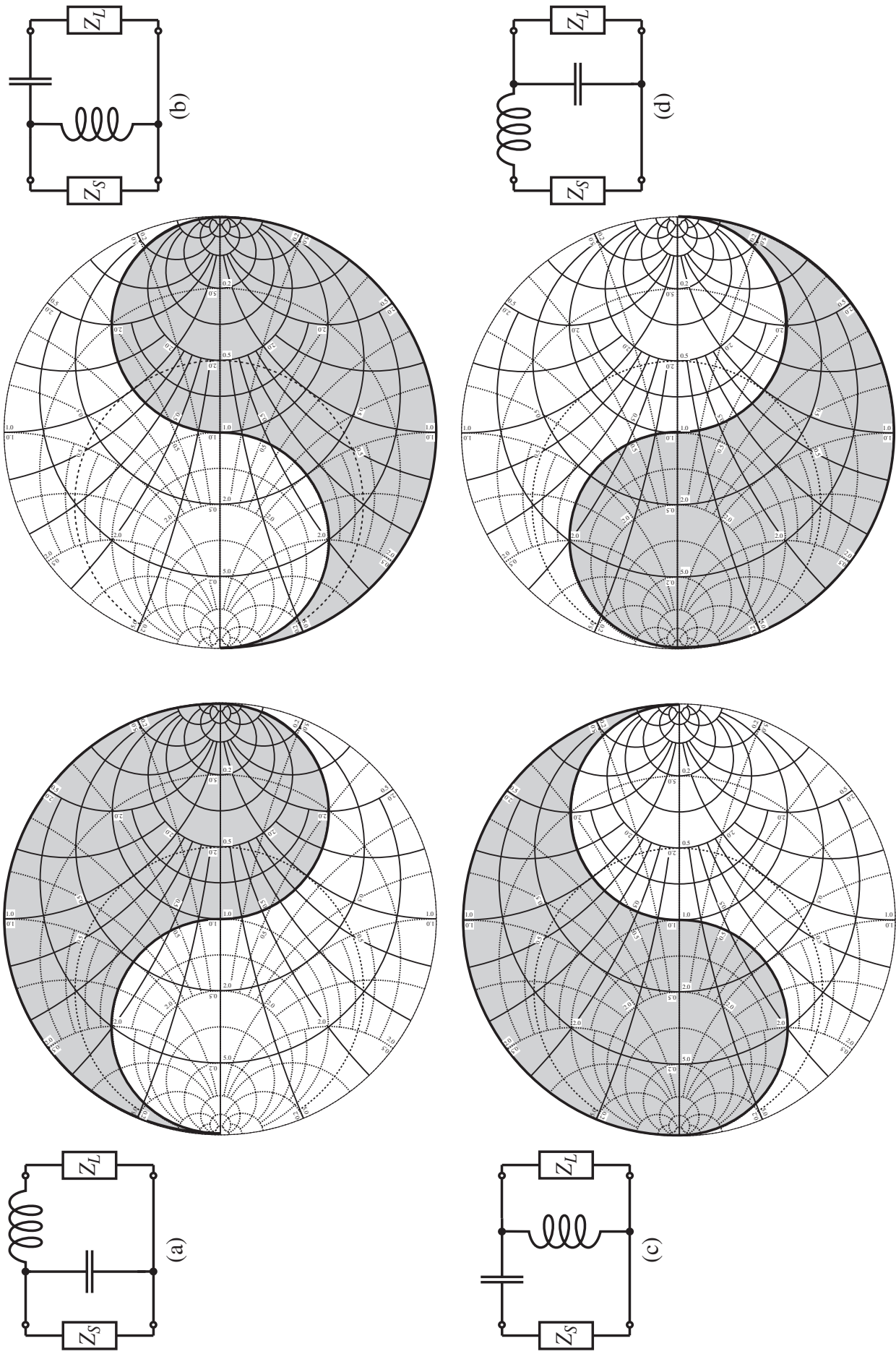
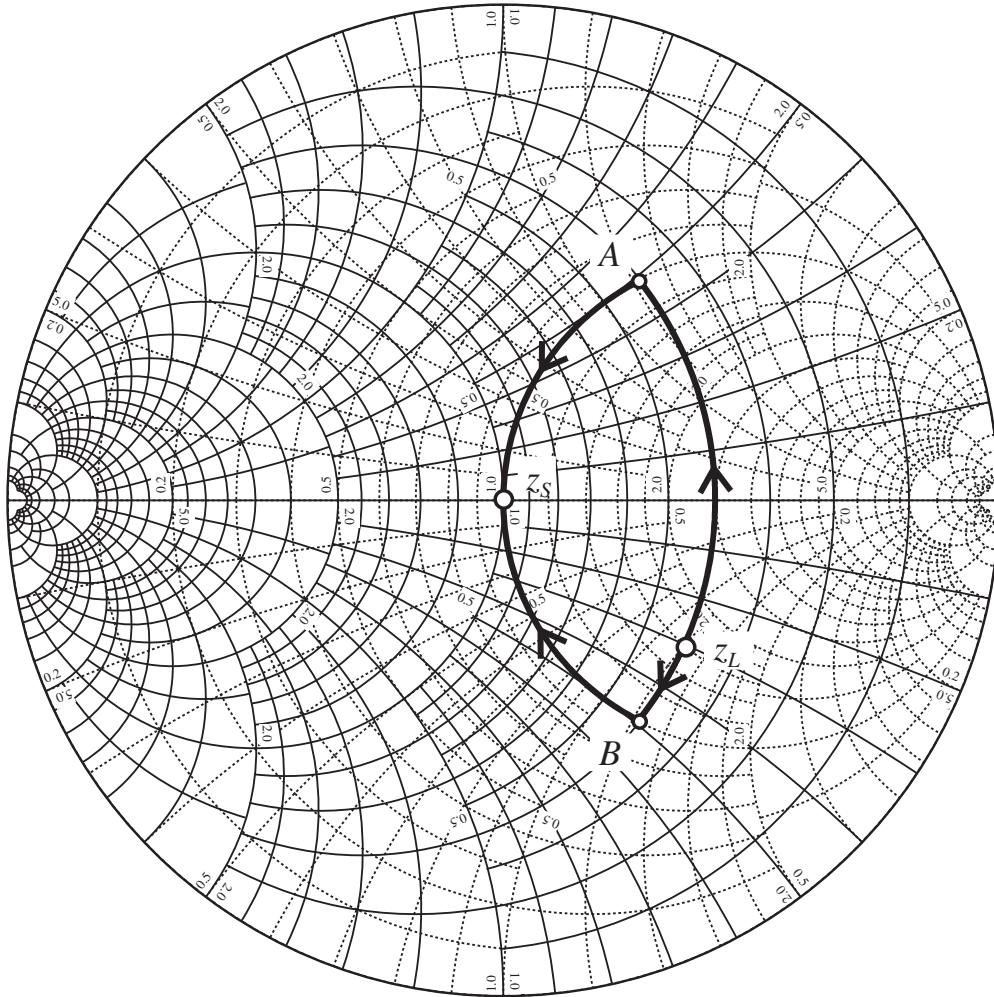
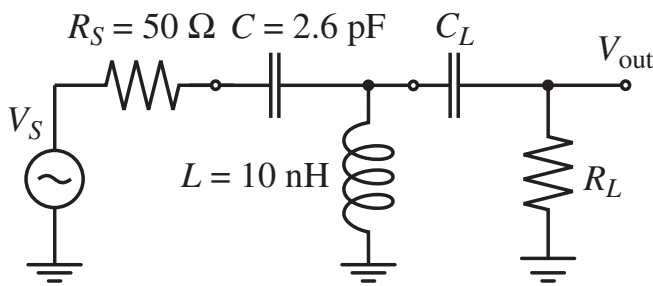


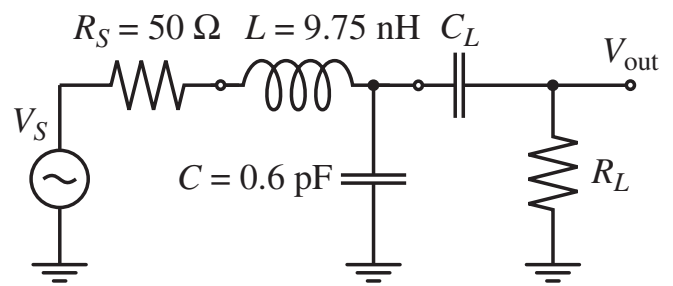
Figure 8-7 Forbidden regions for L-type matching networks with $Z_S = Z_0 = 50 \Omega$.



(a) Impedance transformations displayed in Smith Chart

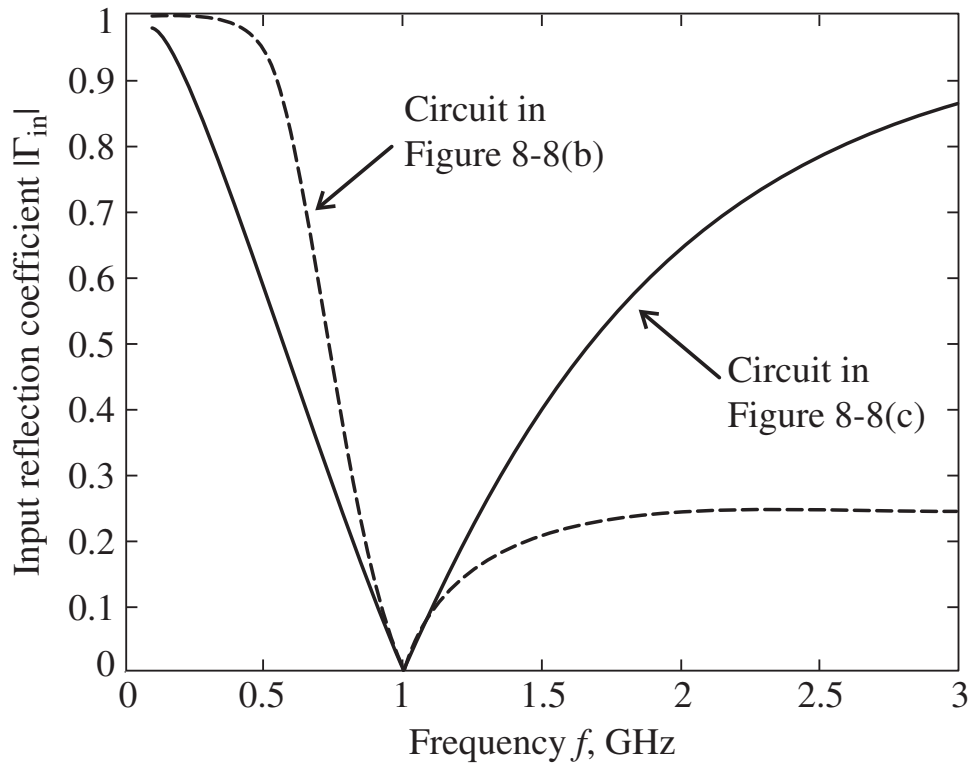


(b)

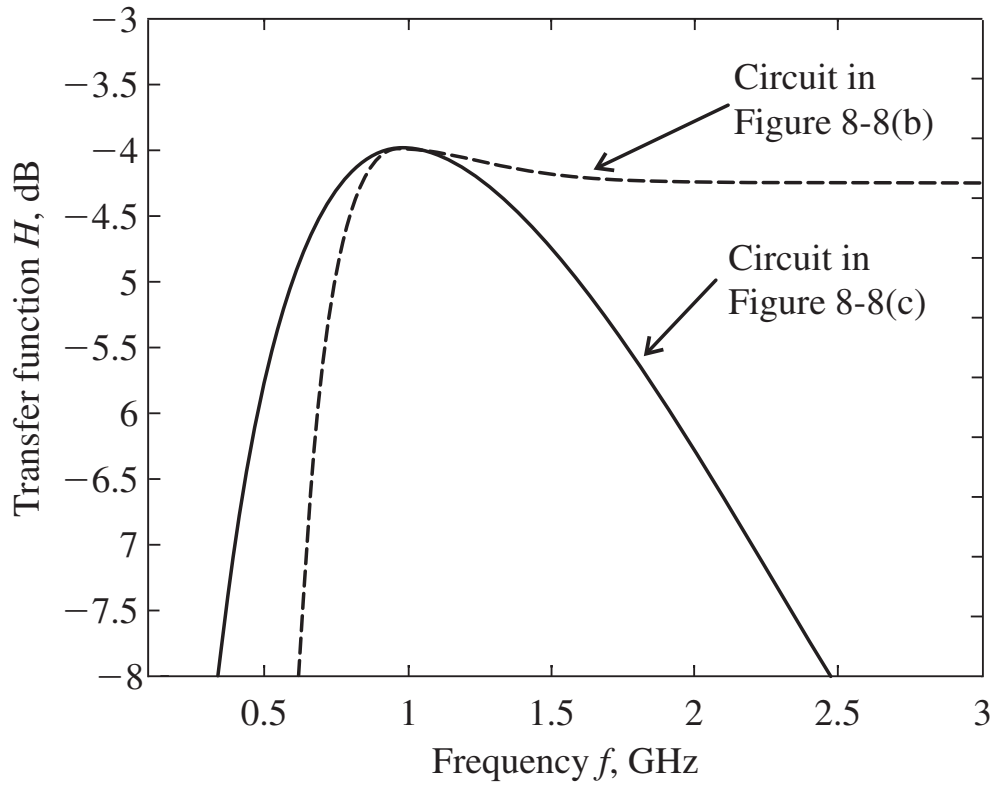


(c)

Figure 8-8 Two design realizations of an L-type matching network.

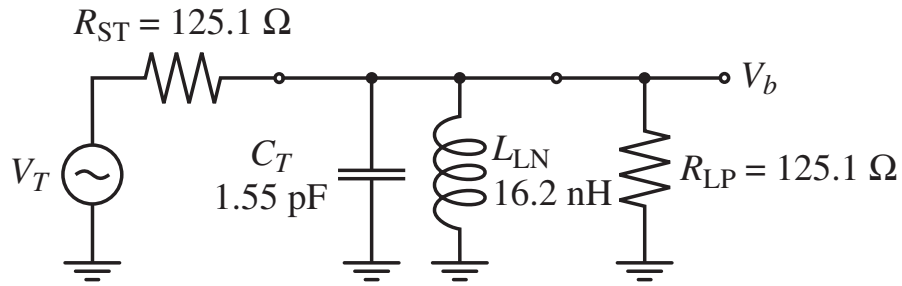


(a) Frequency response of input reflection coefficient

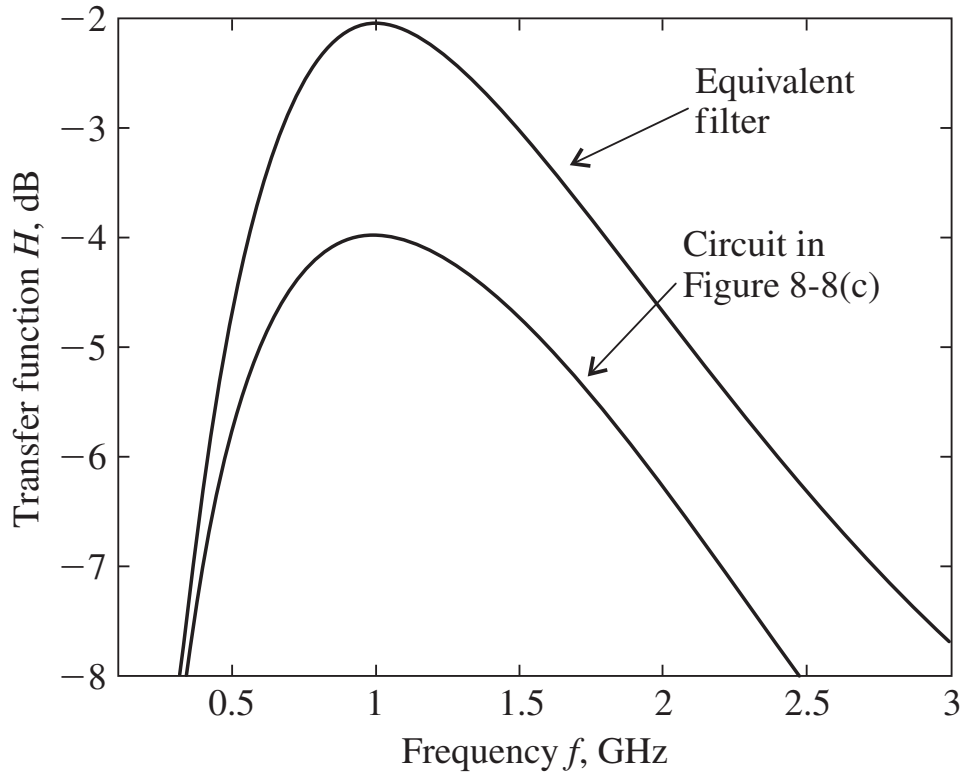


(b) Transfer function of the matching networks

Figure 8-9 Frequency response of the two matching network realizations.



(a) Equivalent bandpass filter



(b) Frequency response of the matching network compared to the equivalent filter response

Figure 8-10 Comparison of the frequency response of the L-type matching network and an equivalent bandpass filter.

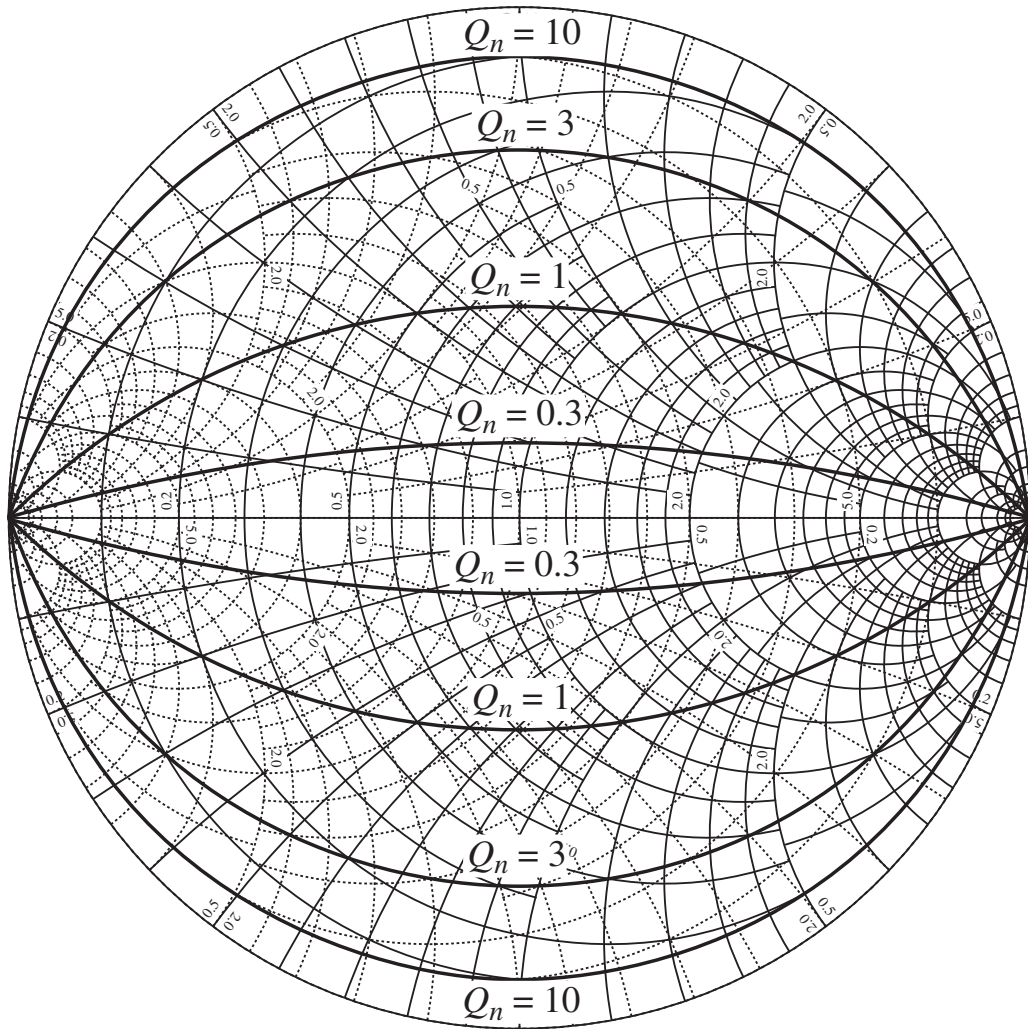
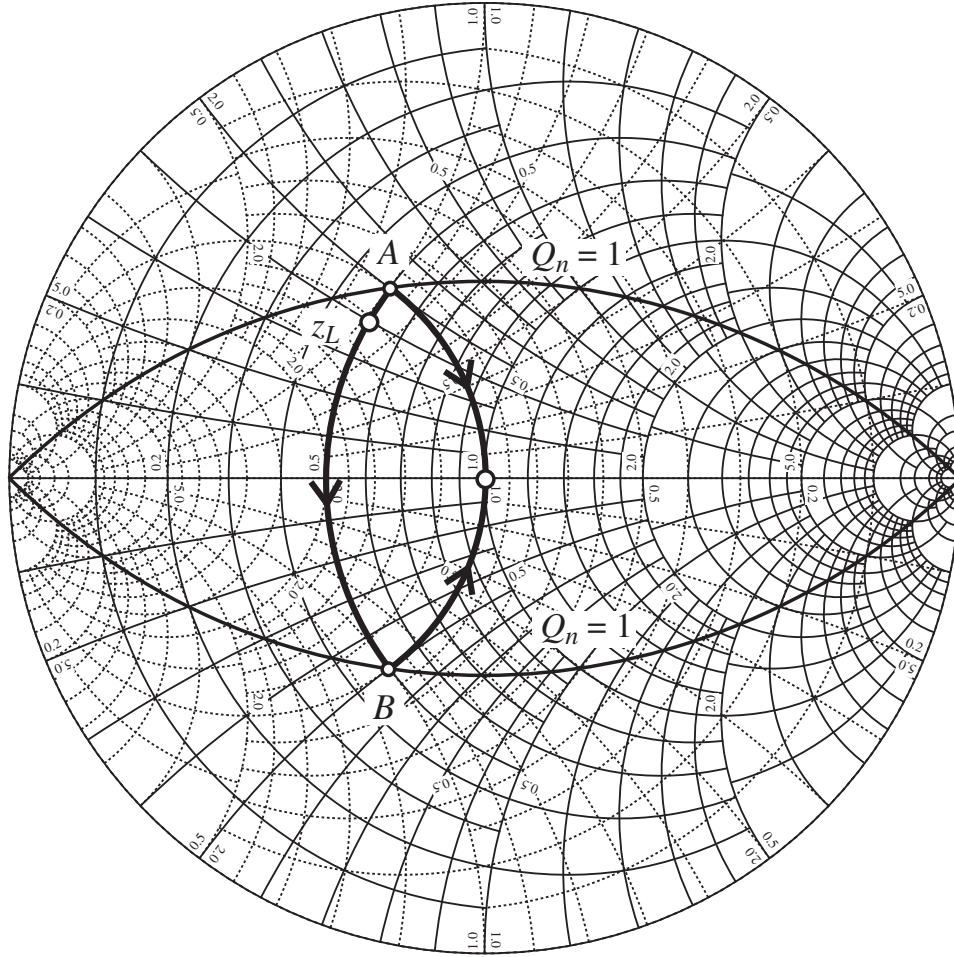
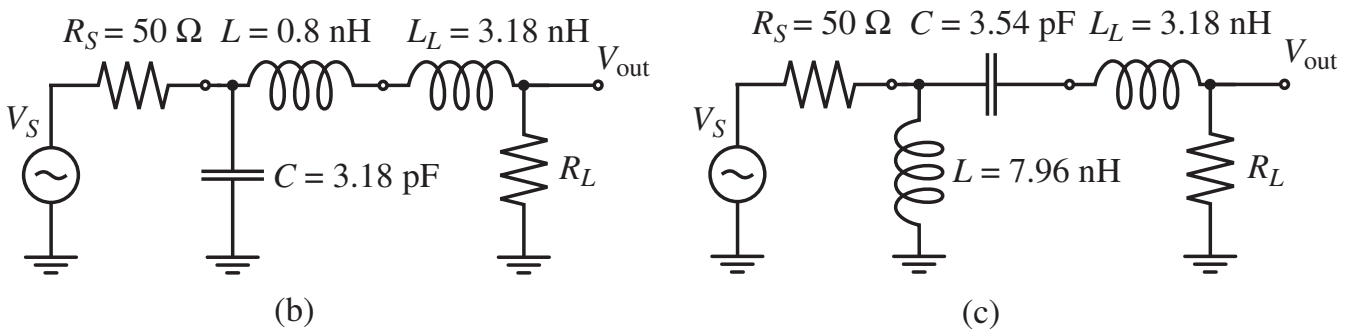


Figure 8-11 Constant Q_n contours displayed in the Smith Chart.



(a) Impedance transformation in the Smith Chart



Resulting matching networks

Figure 8-12 Two L-type matching networks for a 50Ω source and a $Z_L = (25 + j20)\Omega$ load impedance operated at a frequency of 1 GHz.

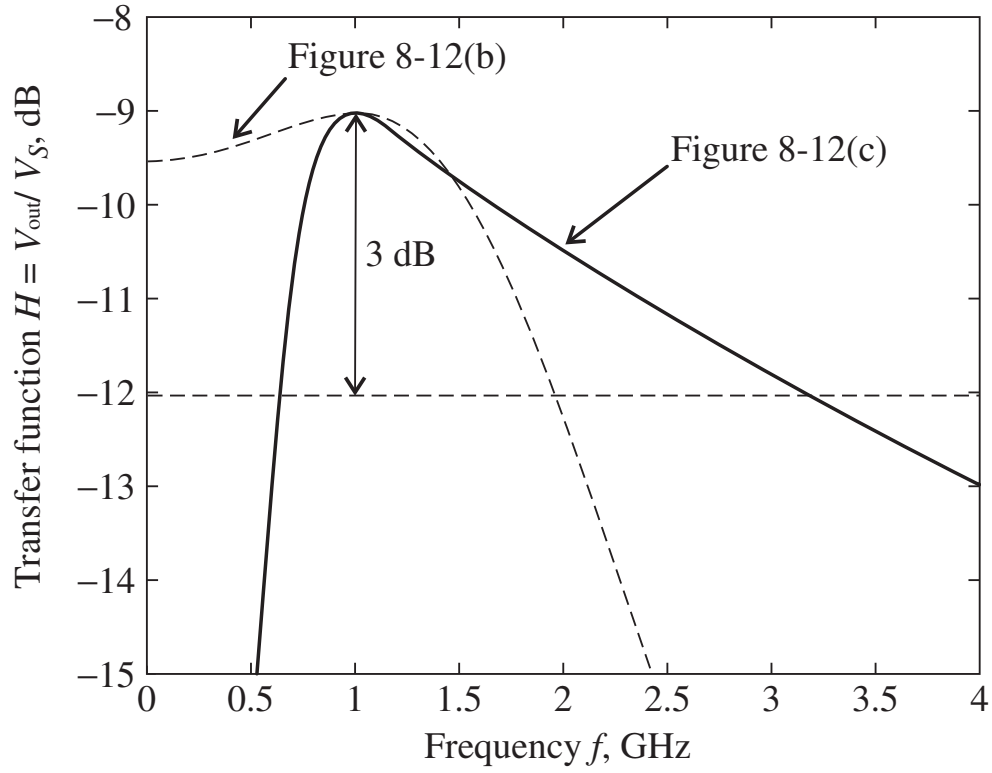


Figure 8-13 Frequency responses for the two matching networks.

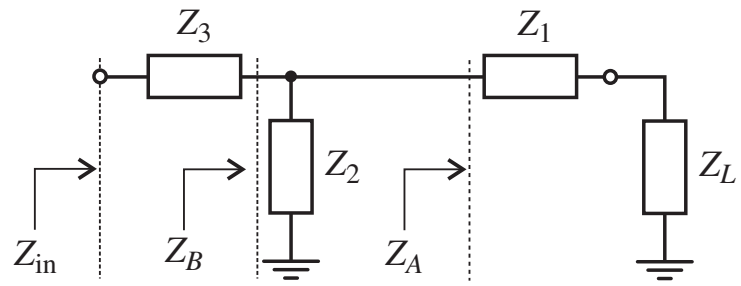


Figure 8-14 General topology of a T-type matching network.

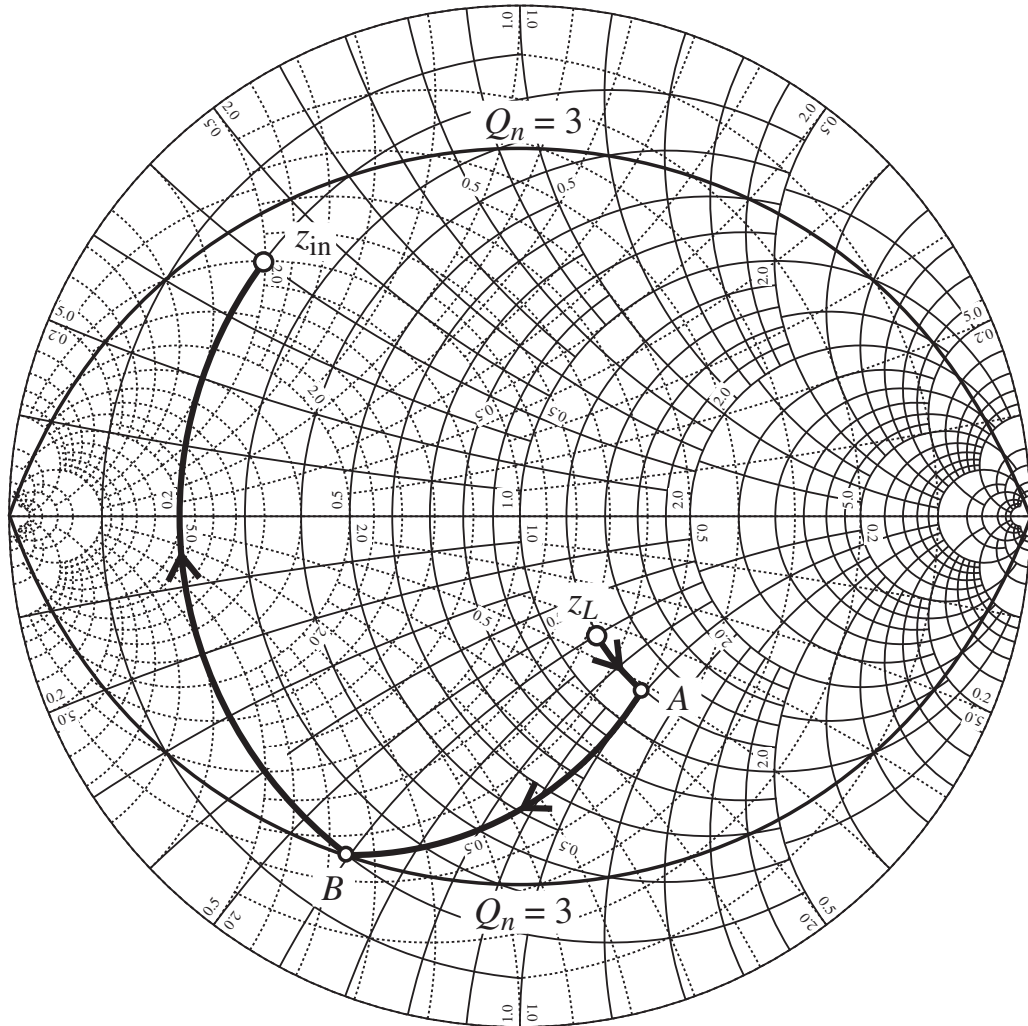


Figure 8-15 Design of a T-type matching network for a specified $Q_n = 3$.

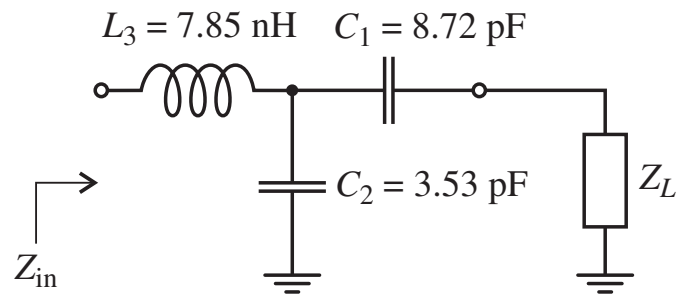


Figure 8-16 T-type matching network circuit schematics.

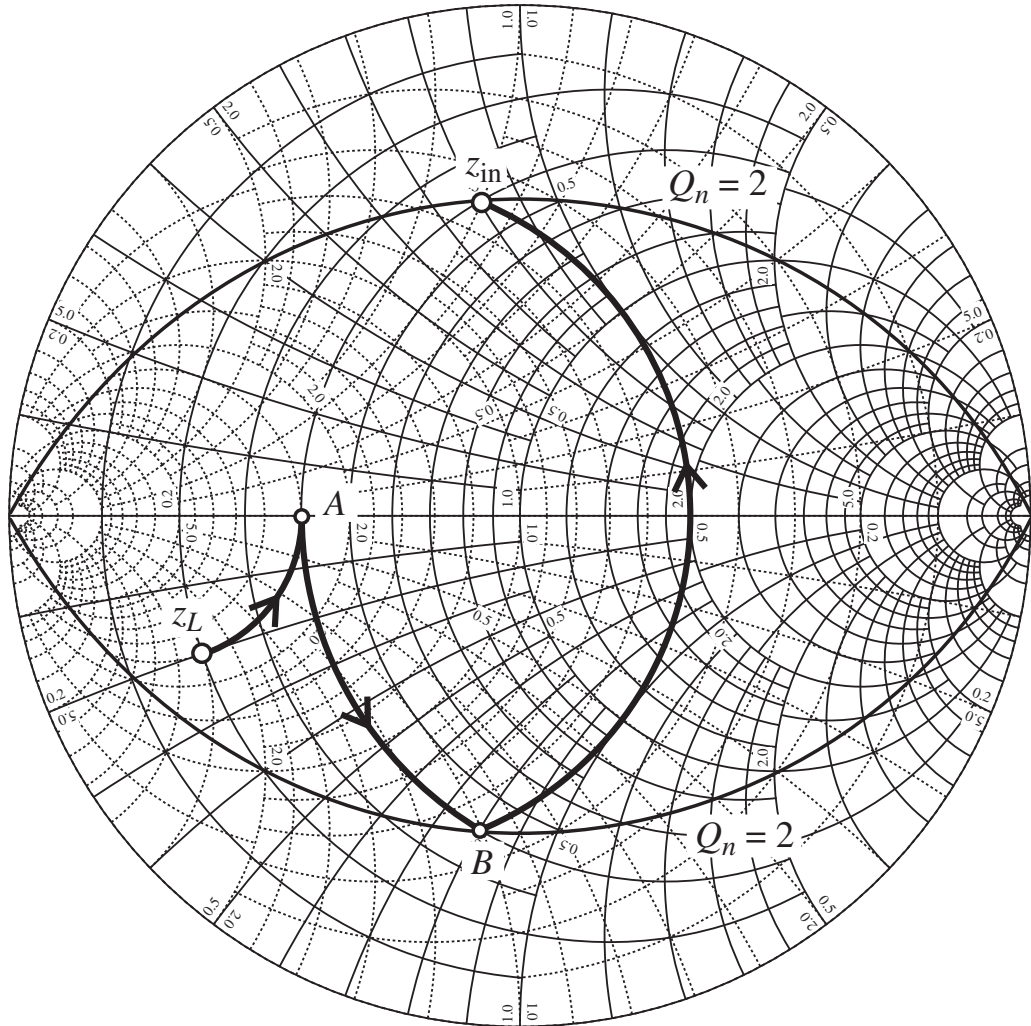


Figure 8-17 Design of a Pi-type matching network using a minimal Q_n .

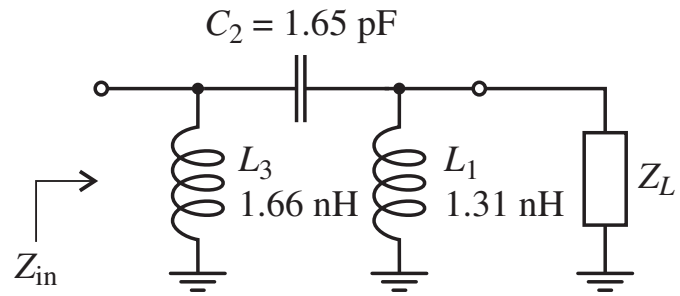


Figure 8-18 Pi-type matching network configuration.

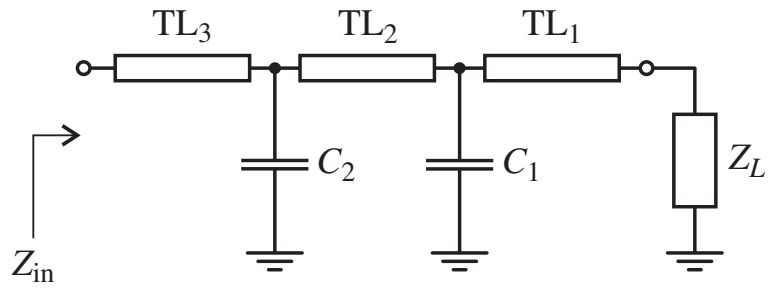


Figure 8-19 Mixed design of matching network involving transmission line sections (TL) and discrete capacitive elements.

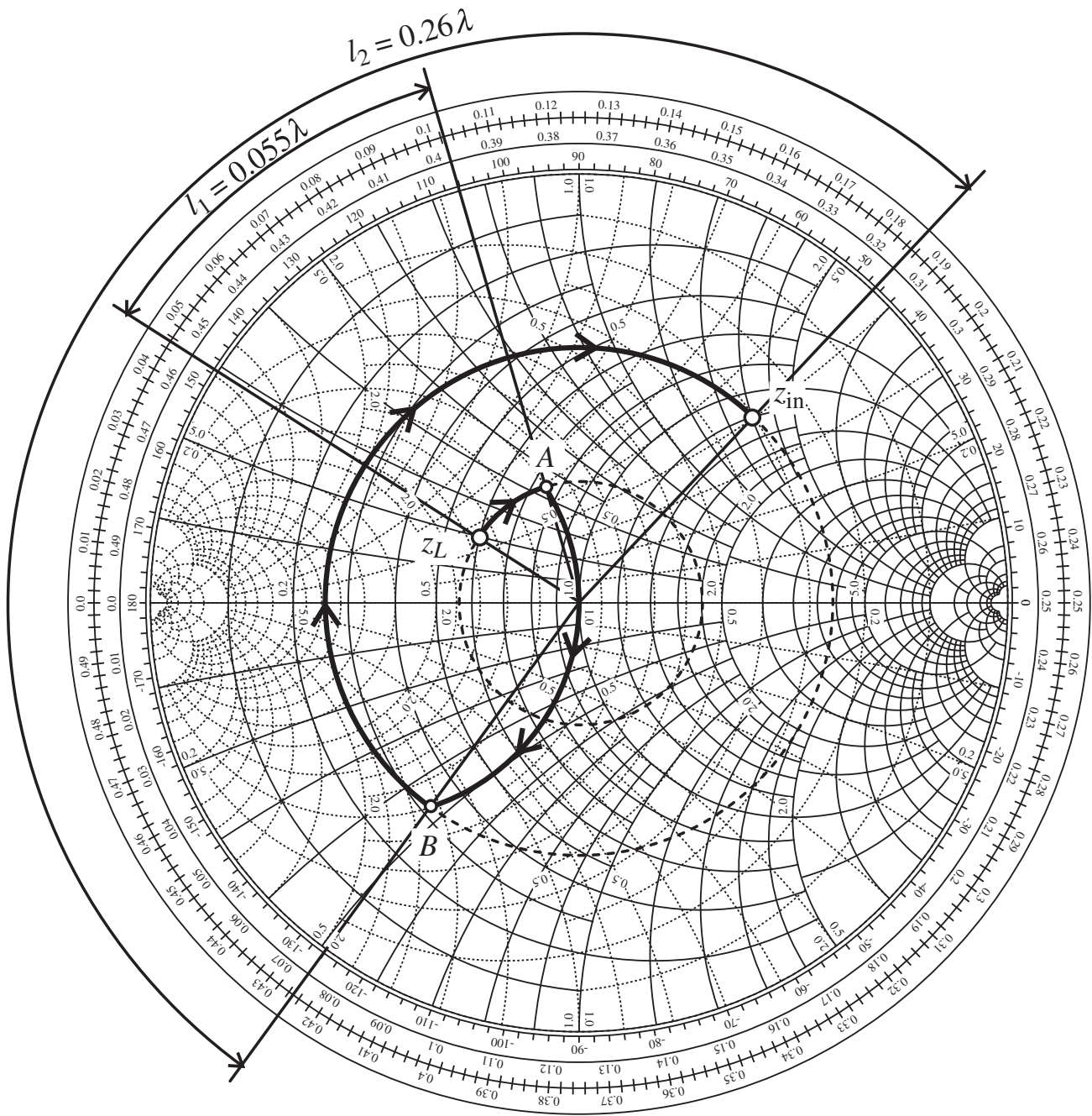


Figure 8-20 Design of the distributed matching network for Example 8-7.

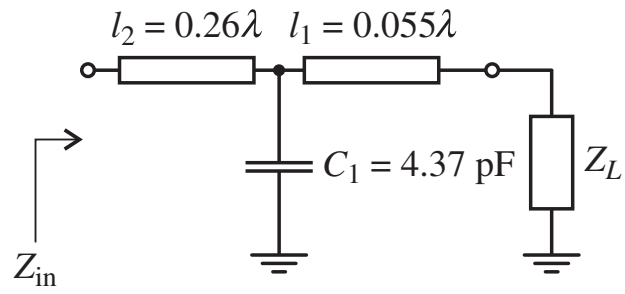


Figure 8-21 Matching network combining series transmission lines and shunt capacitance.

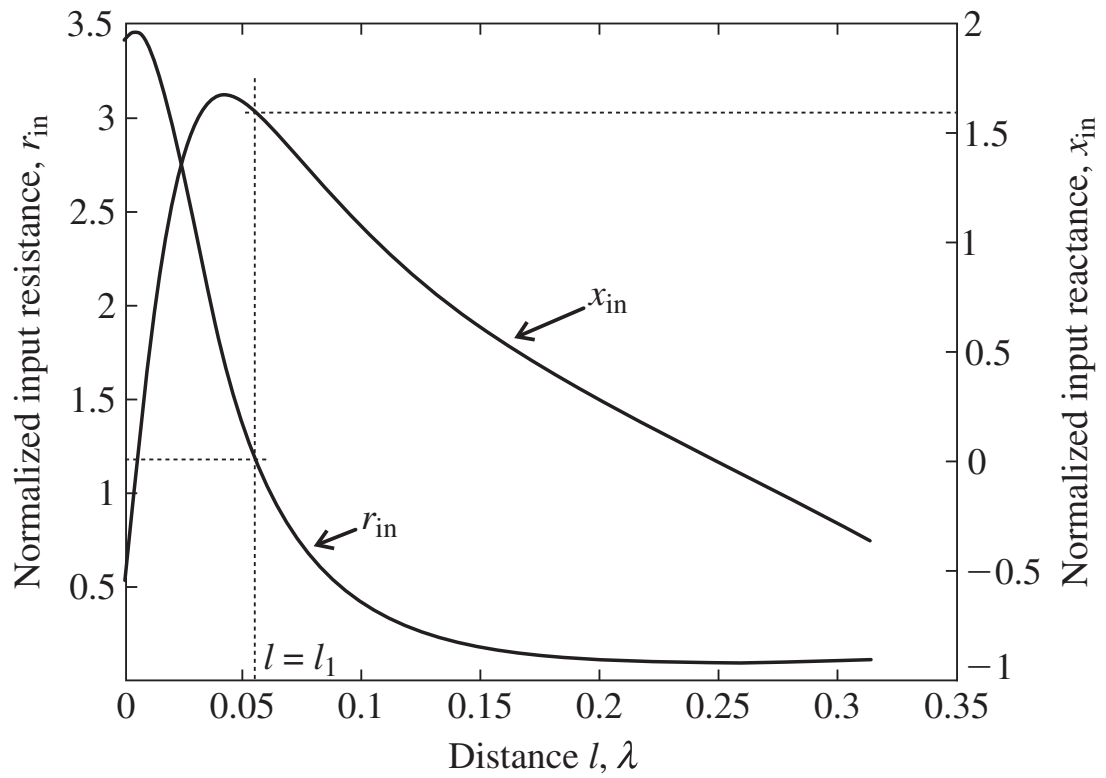


Figure 8-22 Input impedance as a function of the position of the shunt capacitor in Example 8-7.

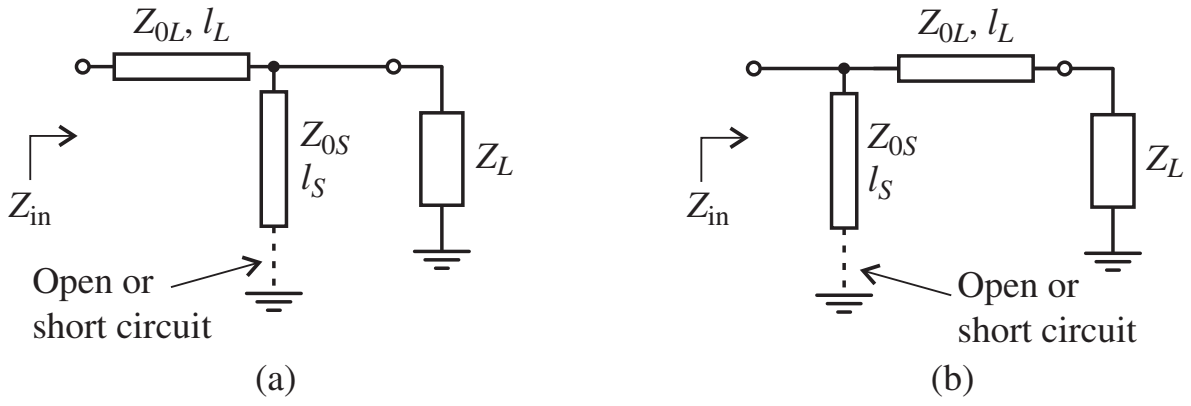


Figure 8-23 Two topologies of single-stub matching networks.

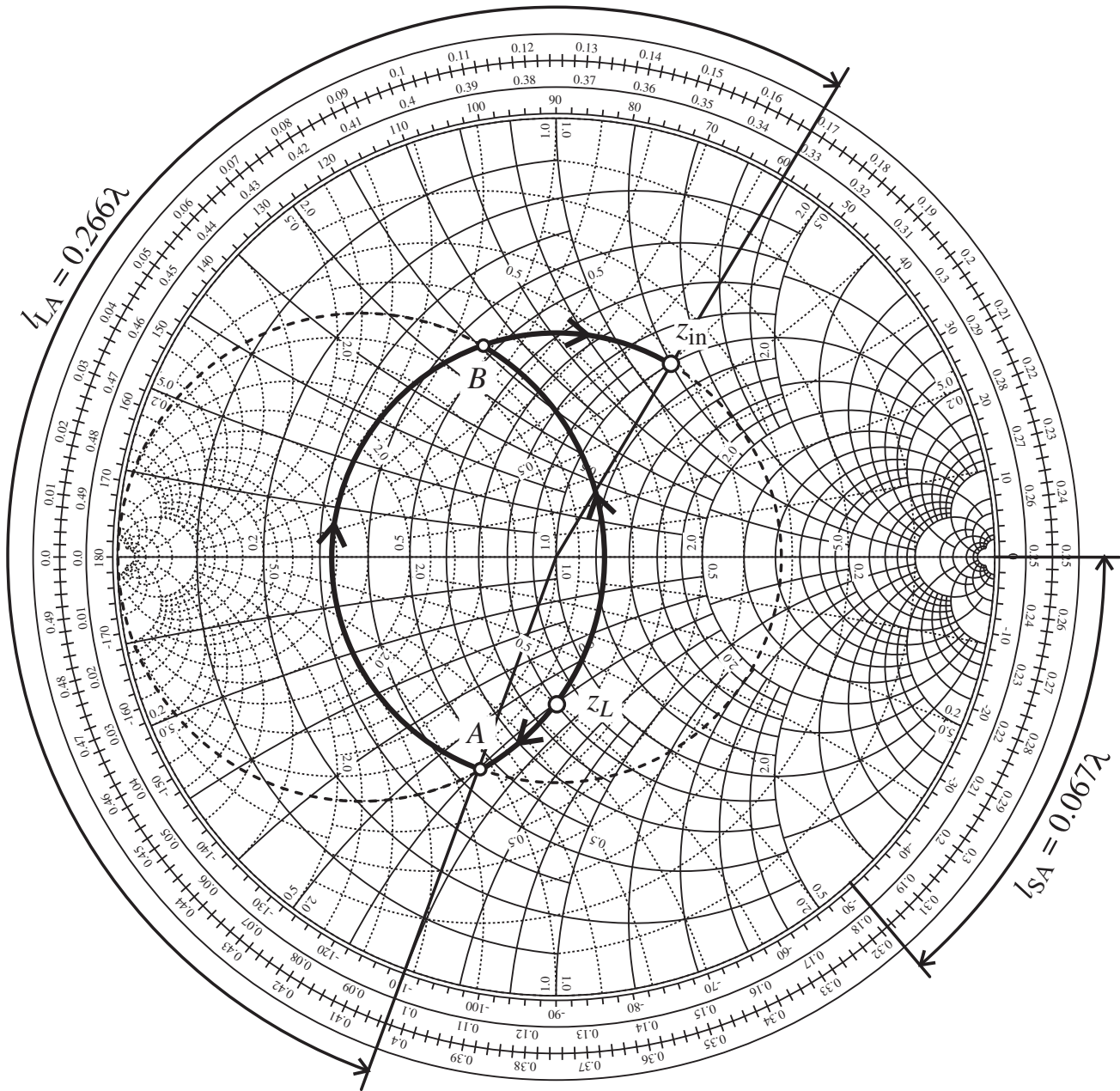


Figure 8-24 Smith Chart design for the single-stub matching network based on Example 8-8.

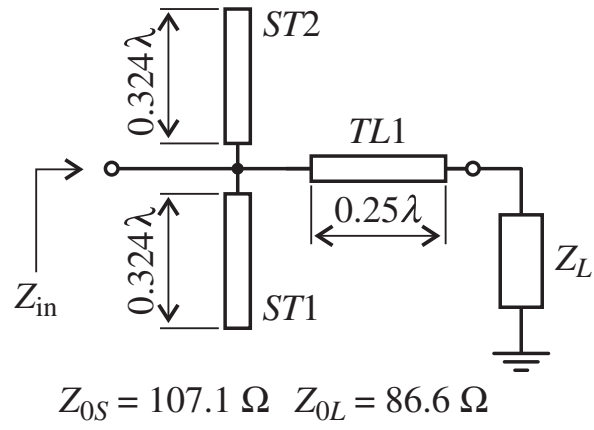


Figure 8-25 Balanced stub design for Example 8-9.

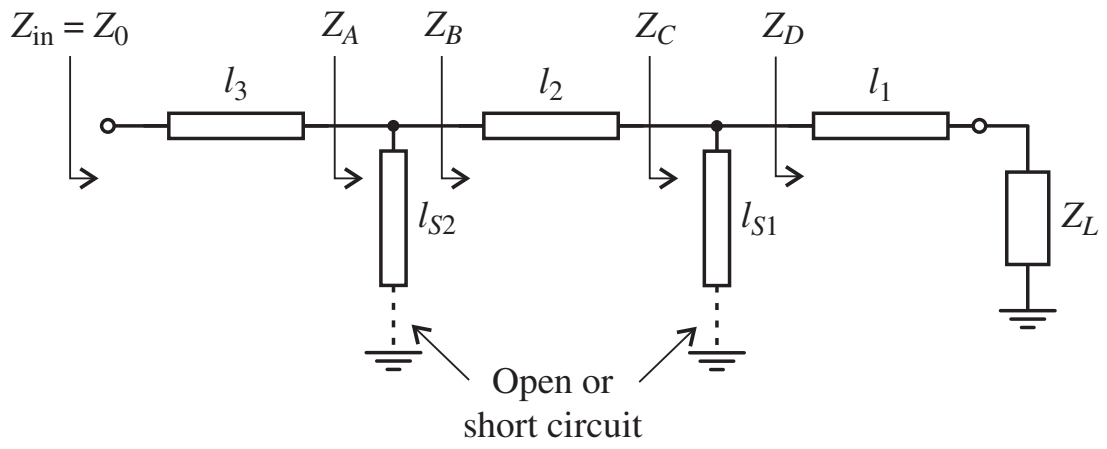


Figure 8-26 Double-stub matching network arrangement.

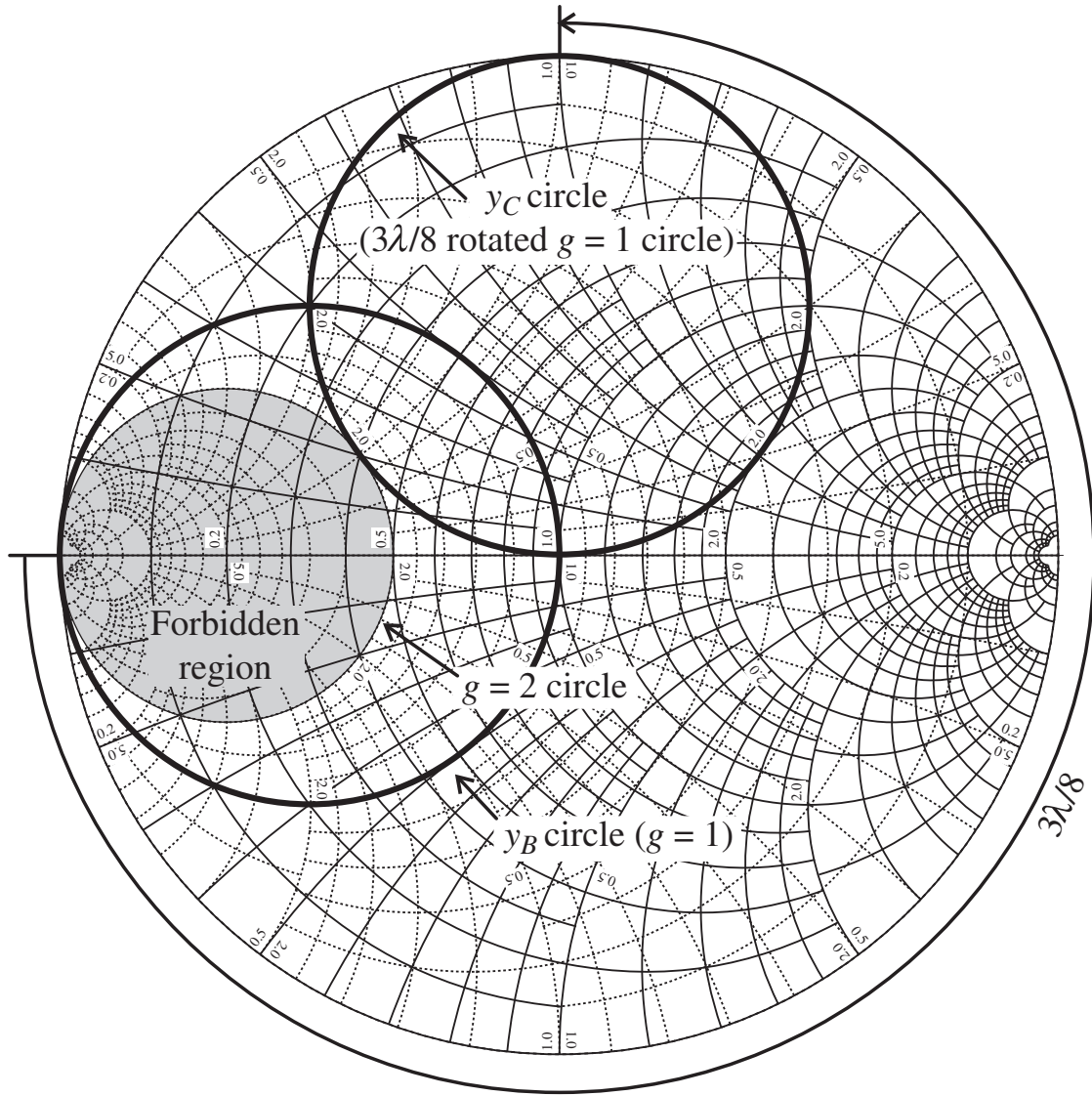


Figure 8-27 Smith Chart analysis of a double-stub matching network shown in Figure 26.

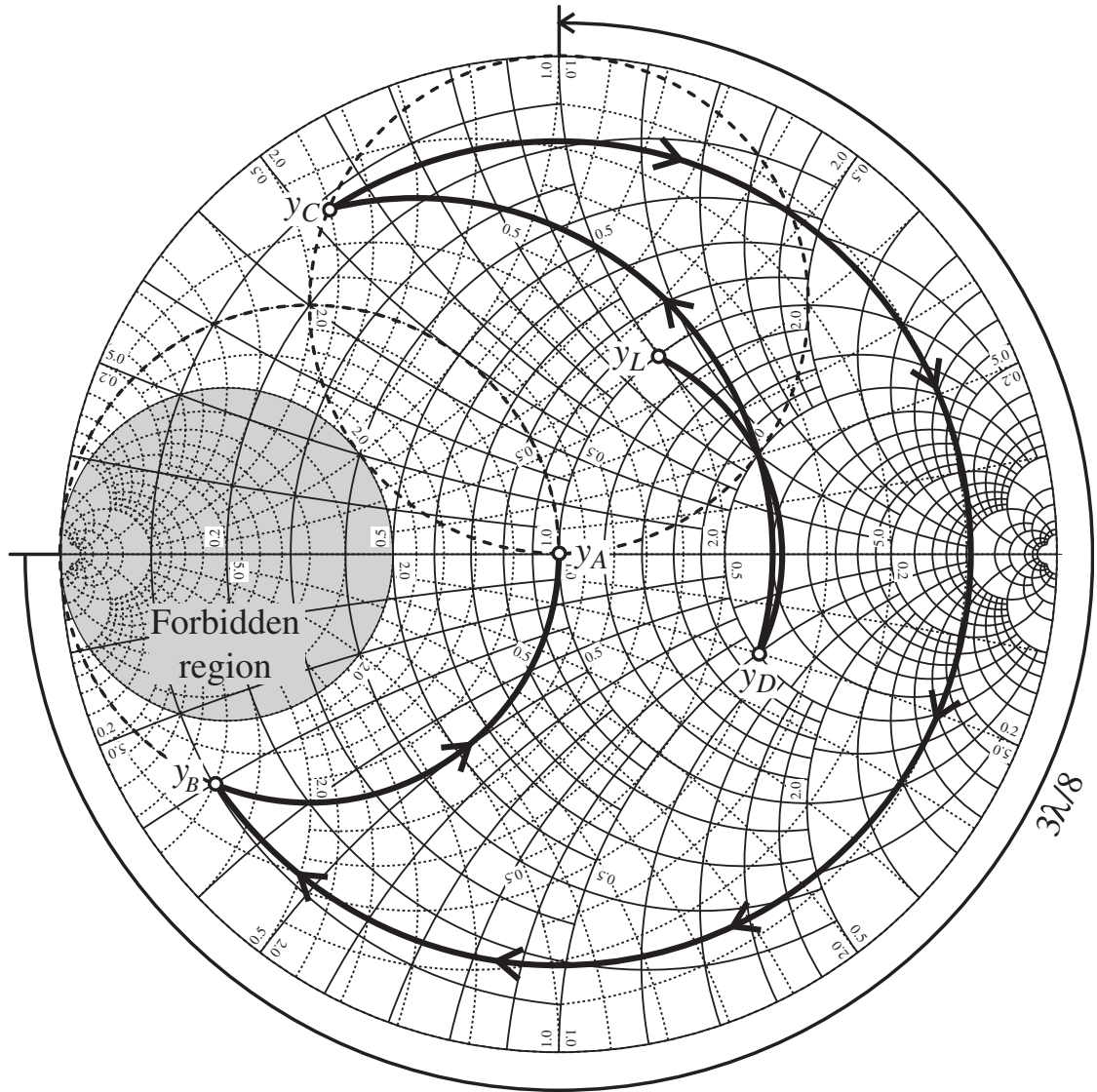


Figure 8-28 Double-stub matching network design for Example 8-10.

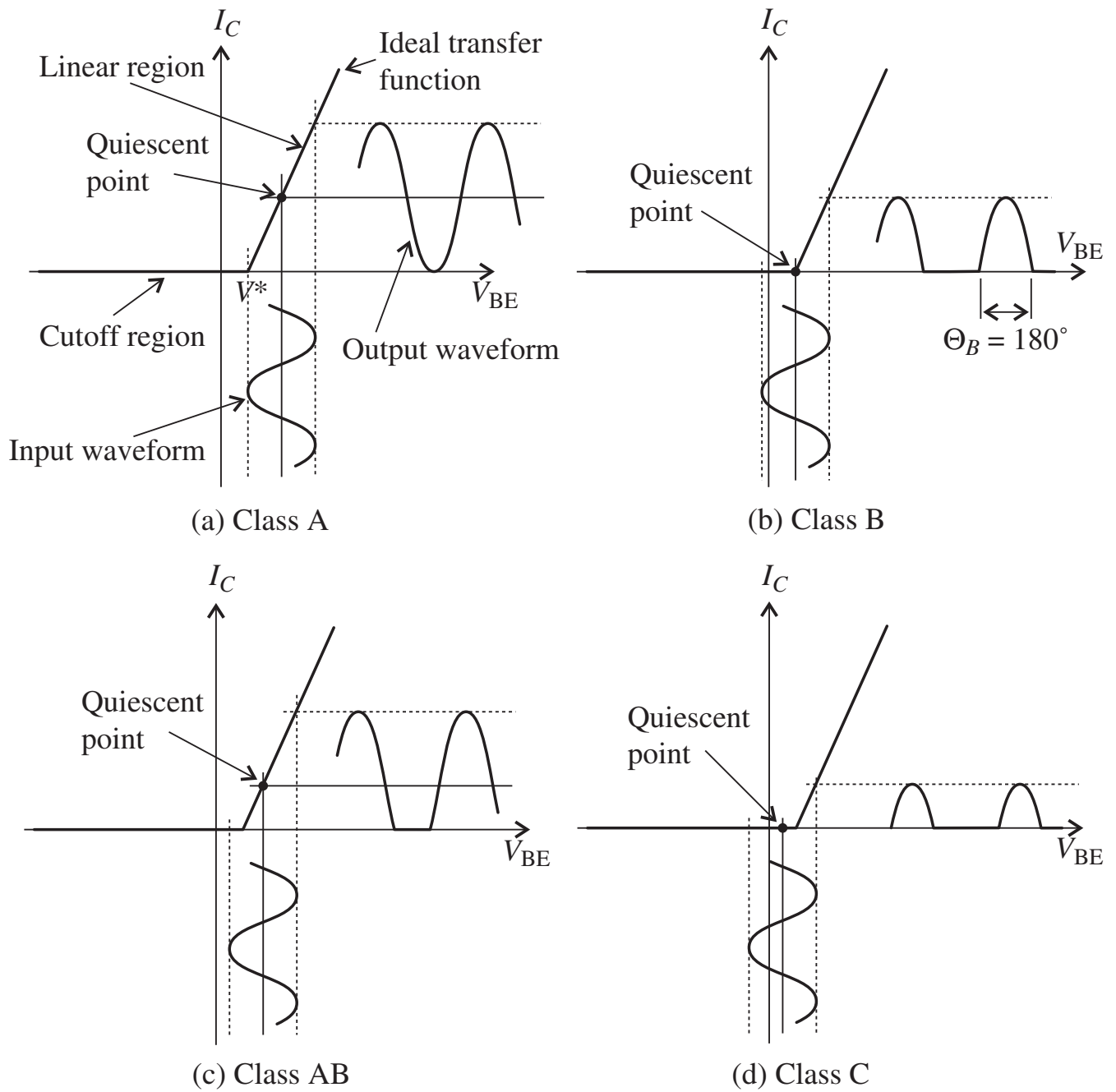
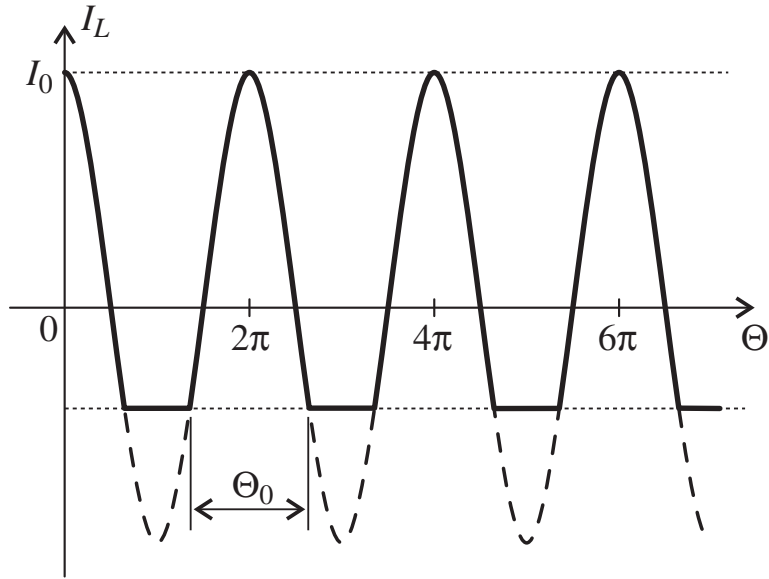
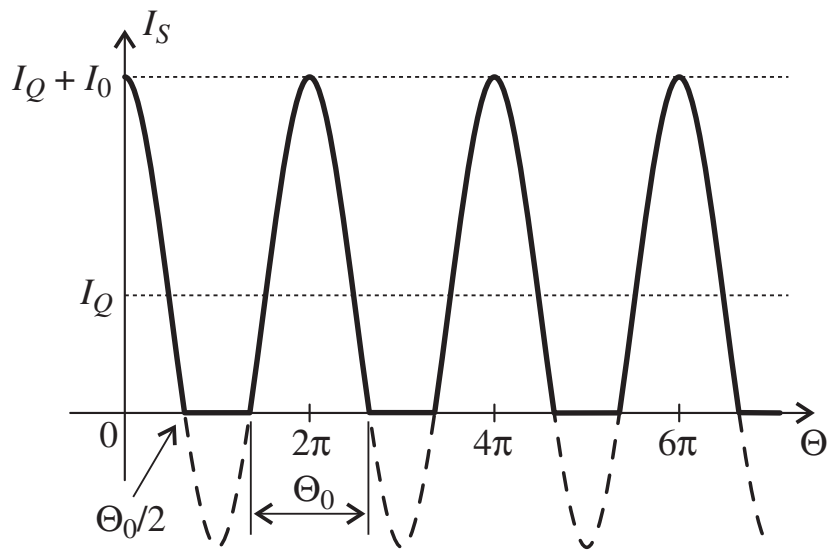


Figure 8-29 Various classes of amplifier operation.



(a) Load current waveform at the output of the transistor



(b) Corresponding power supply current waveform

Figure 8-30 Load and power supply current waveforms as a function of conduction angle.

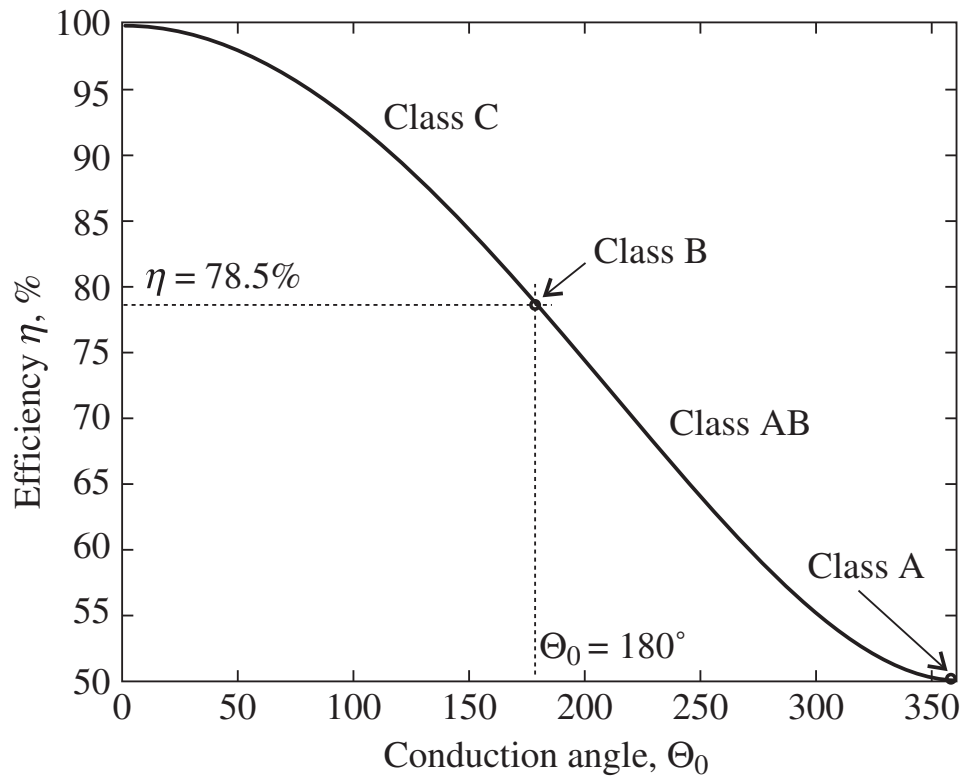


Figure 8-31 Maximum theoretical efficiency of an ideal amplifier as a function of conduction angle.

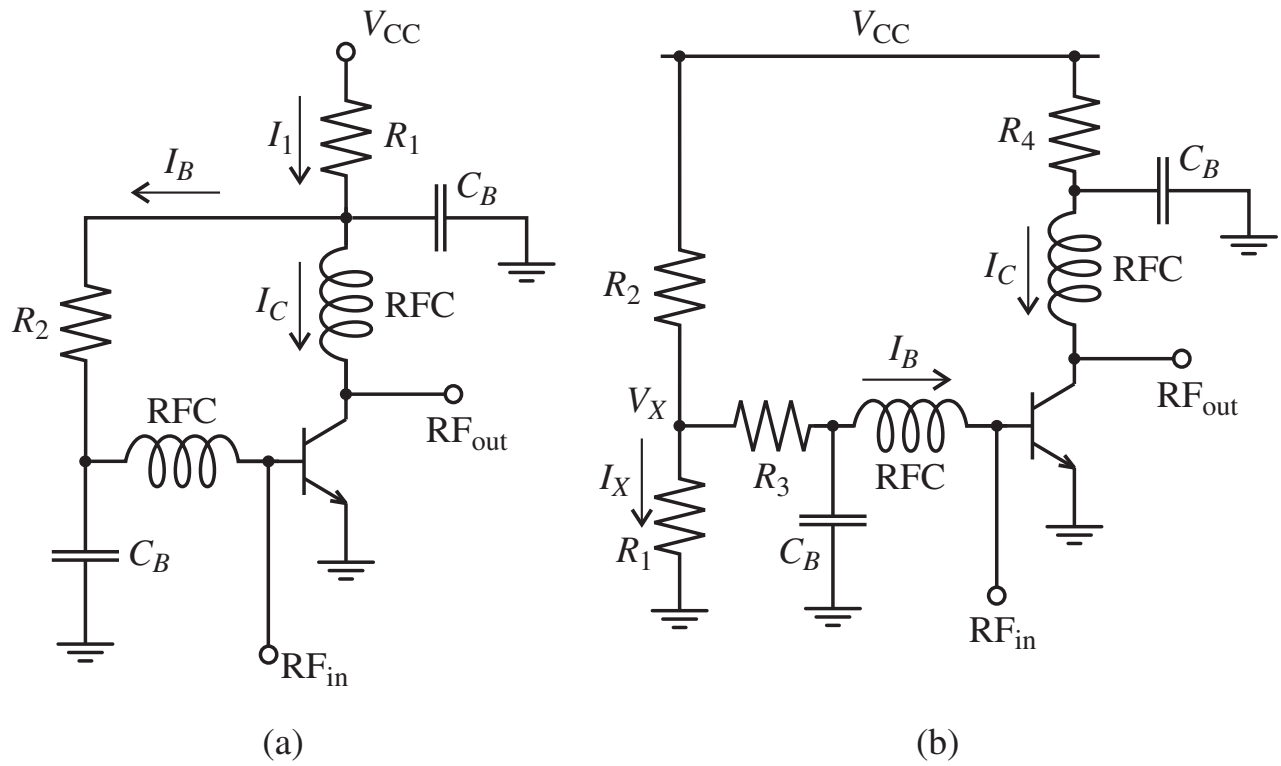


Figure 8-32 Passive biasing networks for an RF BJT in common-emitter configuration.

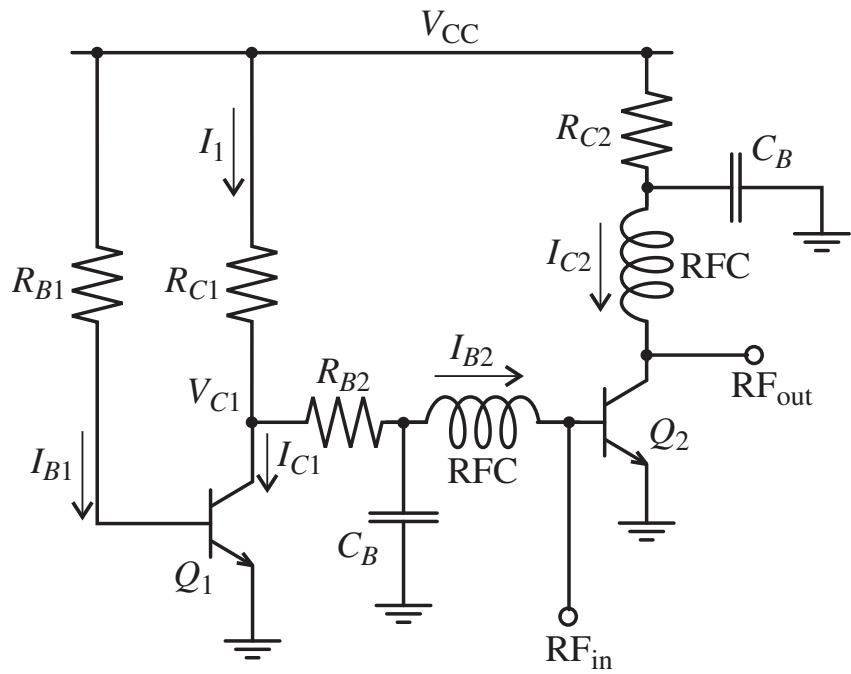


Figure 8-33 Active biasing network for a common-emitter RF BJT.

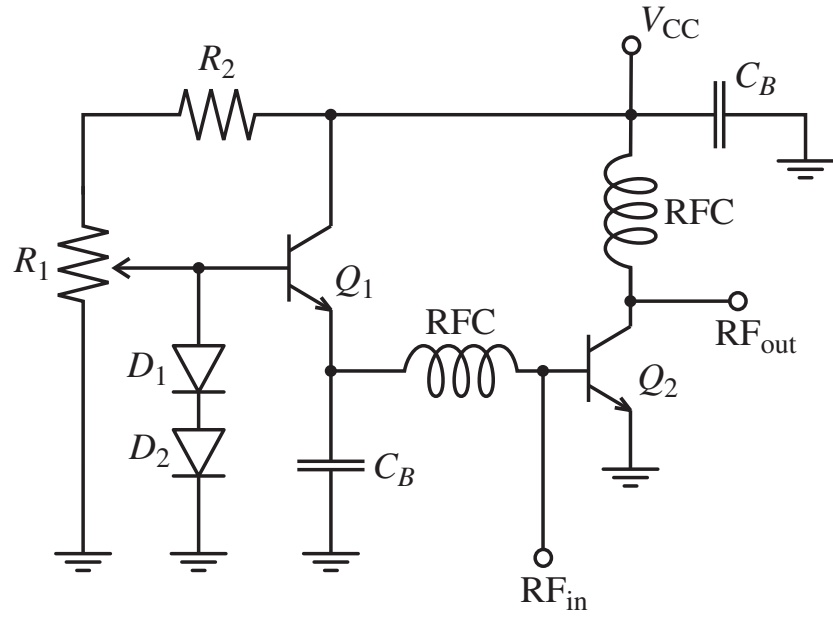


Figure 8-34 Active biasing network containing low-frequency transistor and two diodes.

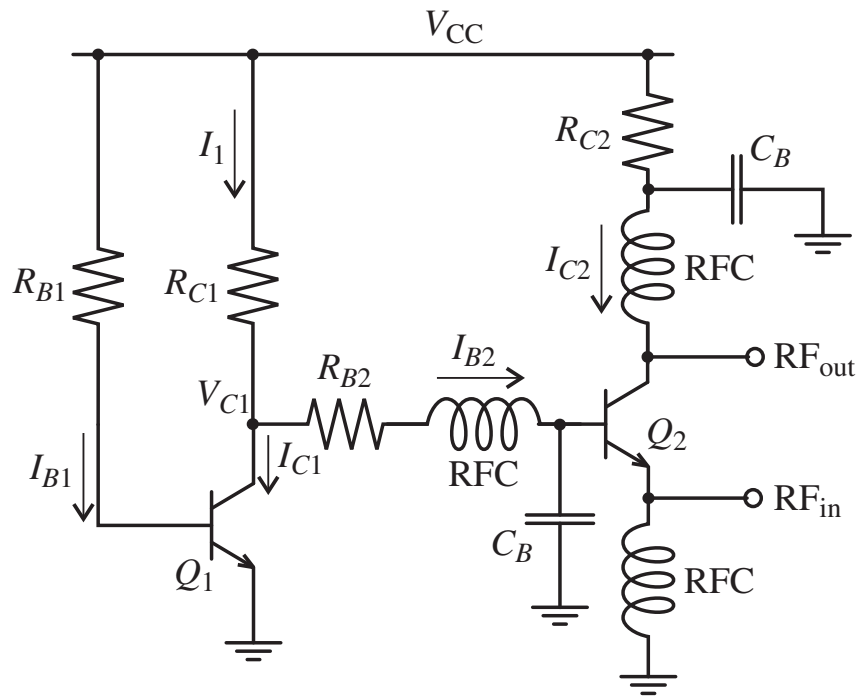


Figure 8-35 Modification of the active biasing network shown in Figure 33 for common-base RF operation.

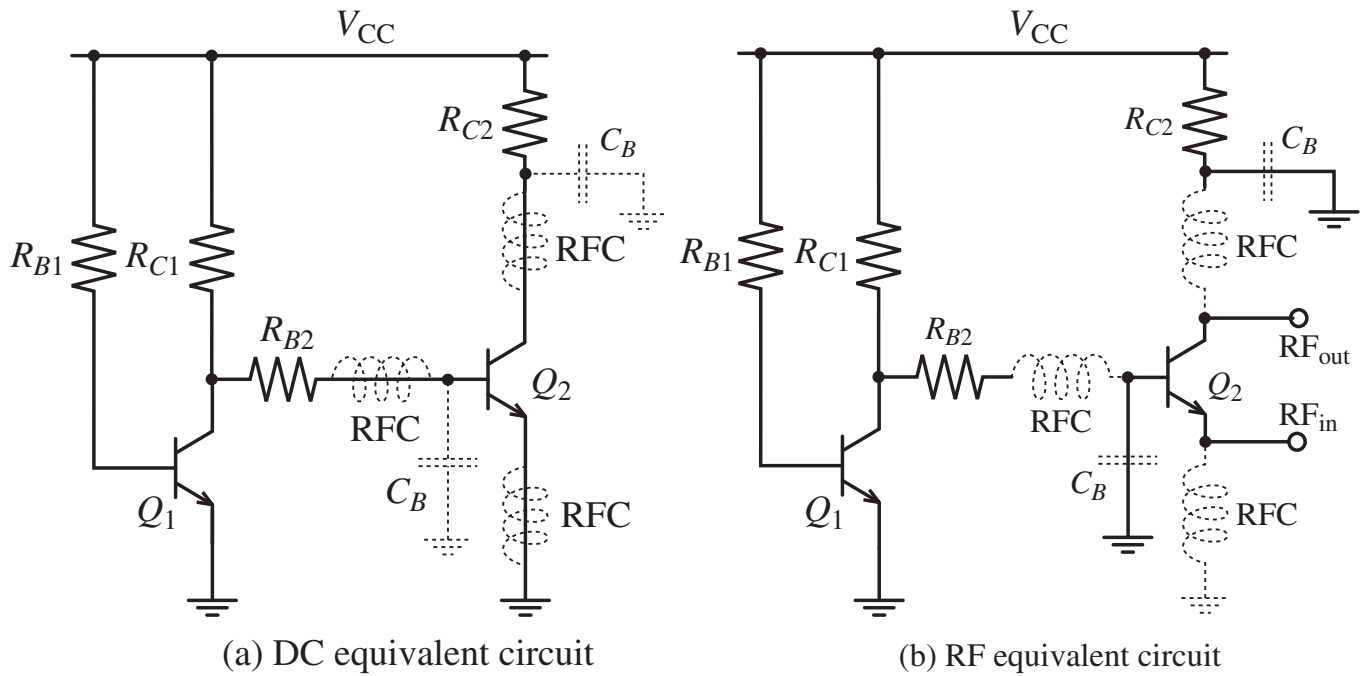


Figure 8-36 DC and RF equivalent circuits for the active biasing network in Figure 35.

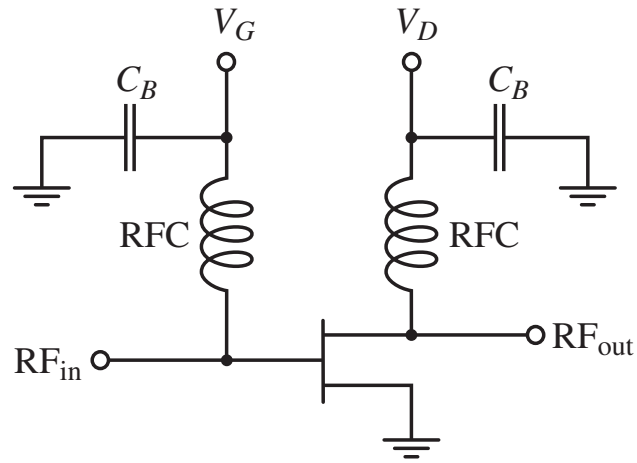


Figure 8-37 Bipolar passive biasing network for FETs.

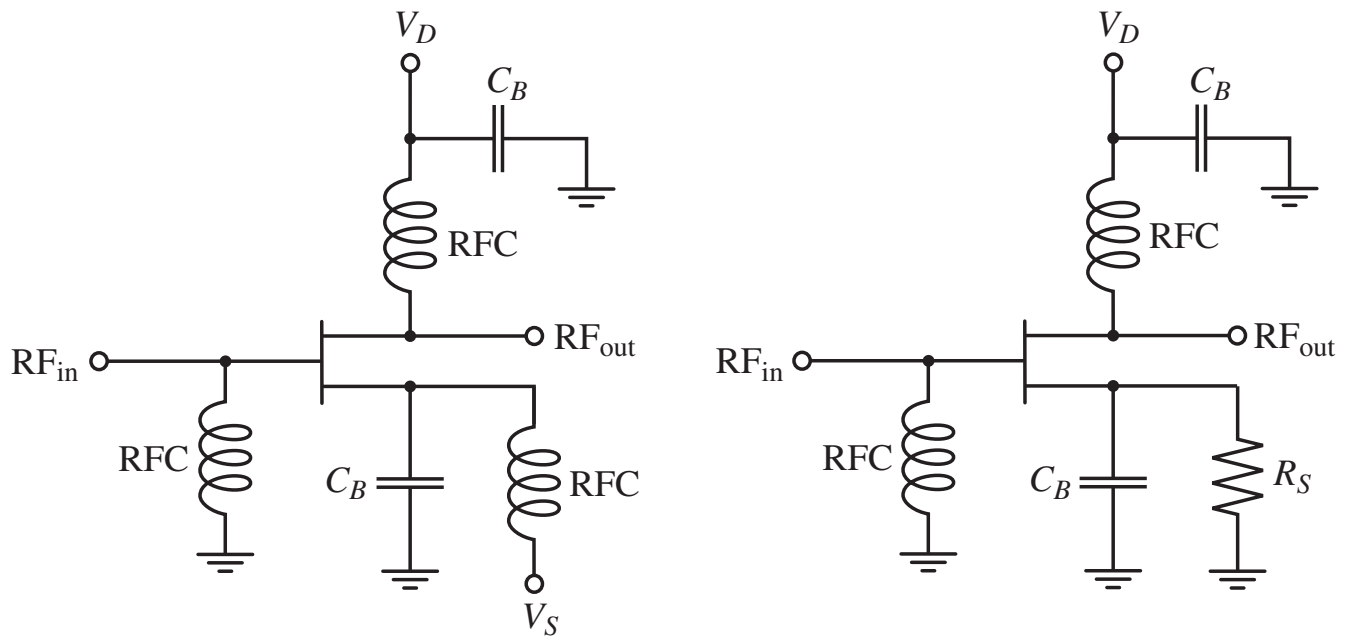


Figure 8-38 Unipolar passive biasing networks for FETs.

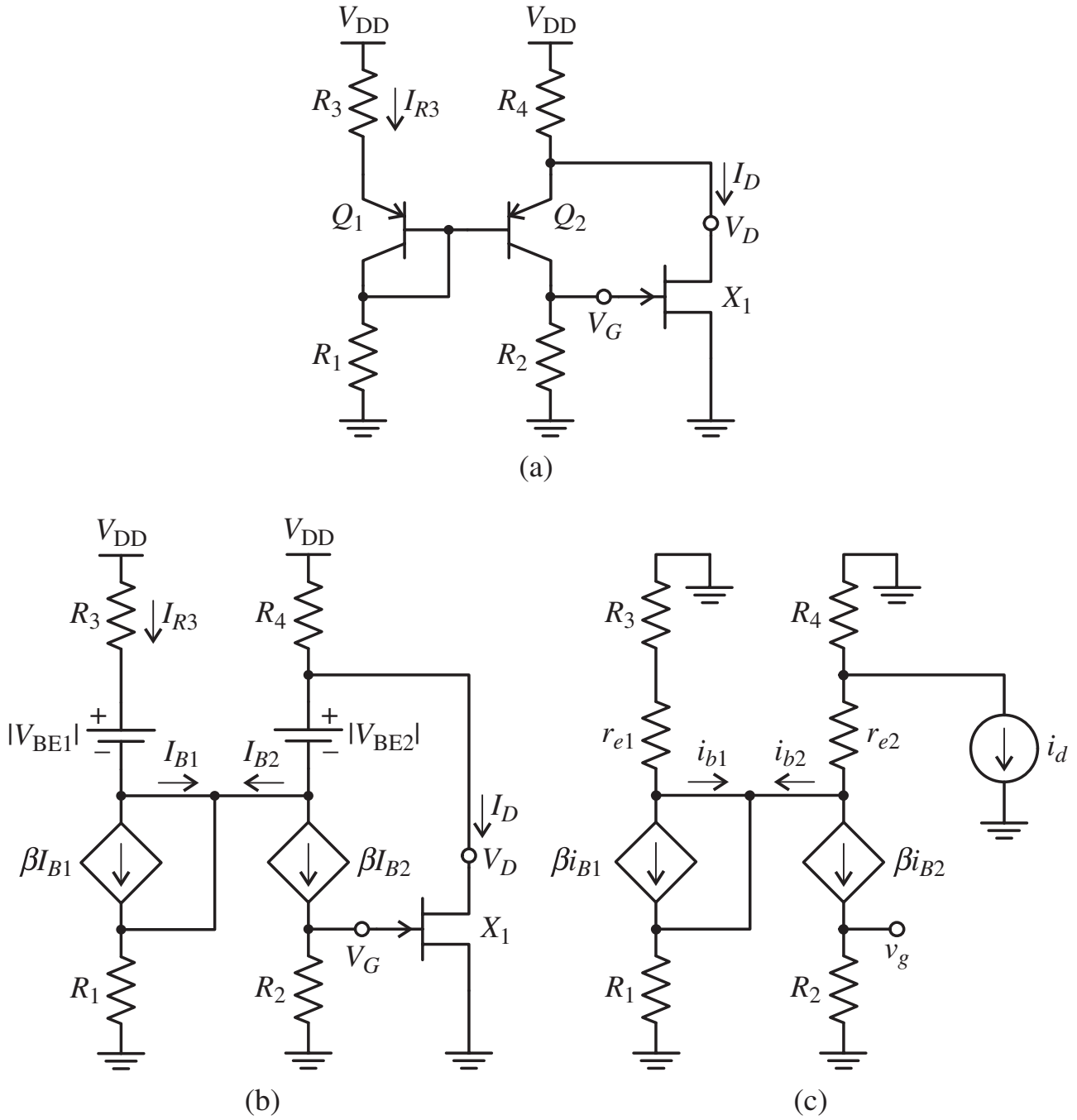


Figure 8-39 E-PHEMT biasing network: (a) DC bias circuit, (b) DC model, (c) low-frequency small-signal model.

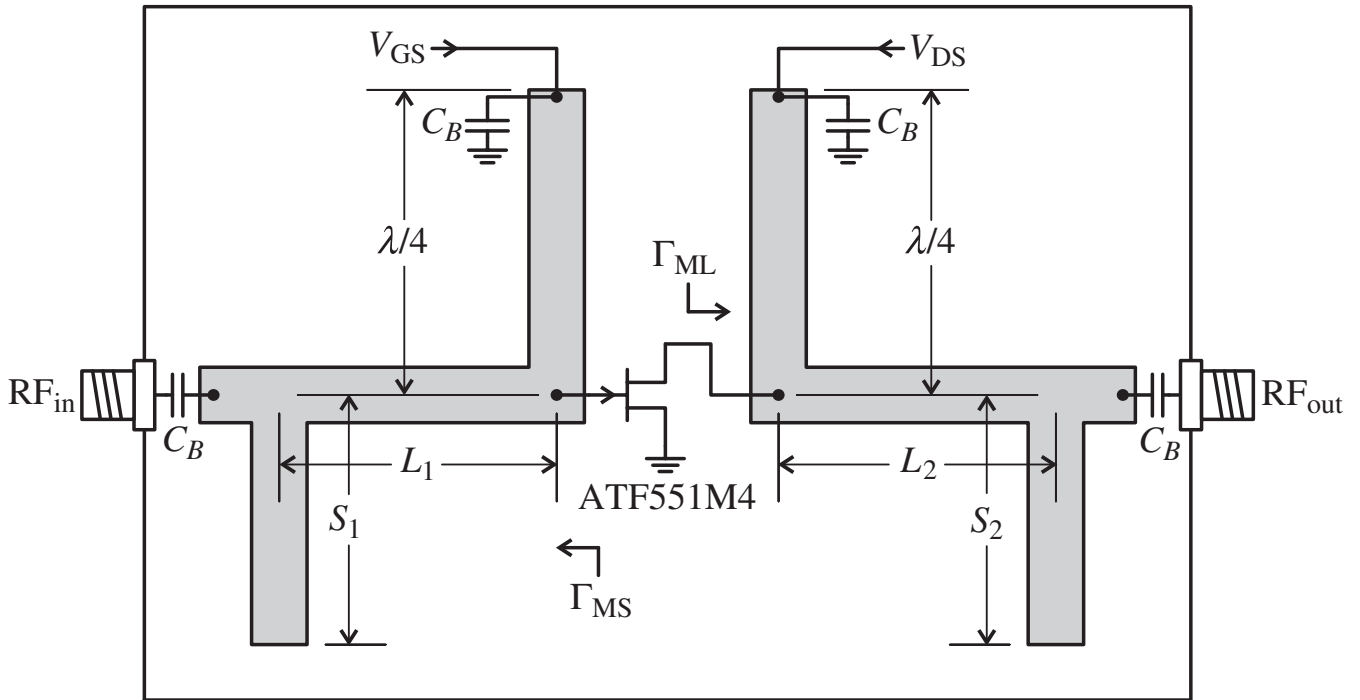
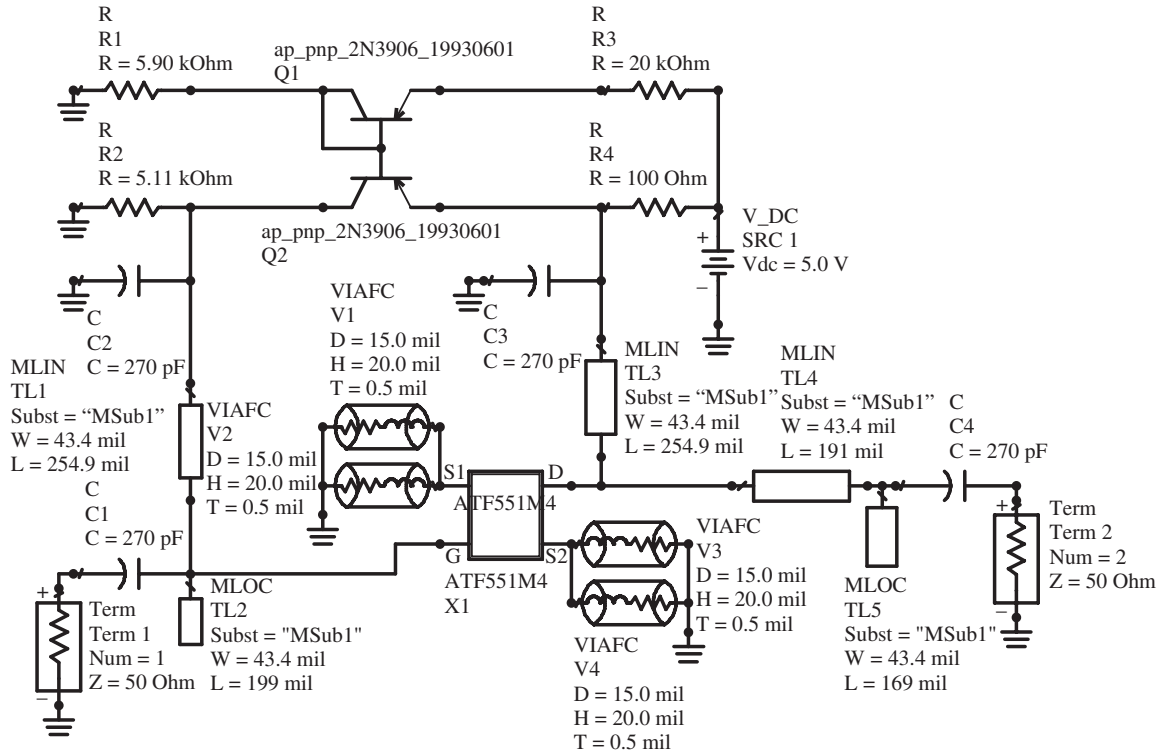


Figure 8-40 Conceptual PCB layout of the 7 GHz amplifier, showing the biasing filters and matching networks implemented with microstrips.



MSub

MSUB
 MSub1
 H = 20.0 mil
 Er = 3.48
 Mur = 1
 Cond = 5.8E + 7
 T = 1.4 mil
 TanD = 0.0031

S-PARAMETERS

S_Param
 SP1
 Start = 0.1 GHz
 Stop = 10 GHz
 Step = 0.01 GHz
 CalcNoise = yas

OPTIONS

Options
 Options 1
 Temp = 16.85
 Tnom = 25
 Topology check = yes
 V_RelTol = 1e-6
 L_RelTol = 1e-6
 GiveAllWarnings = yes
 MaxWarnings = 10

Display Template
 distemp2
 "S_Params_Quad_dB_Smith"
 "S_21_11_wZoom"

Display Template
 distemp3
 "Circles_Ga_NF"
 "Circles_Stability"

Figure 8-41 Schematic of the designed 7 GHz amplifier including the PCB substrate description and the S-parameter simulation setup.

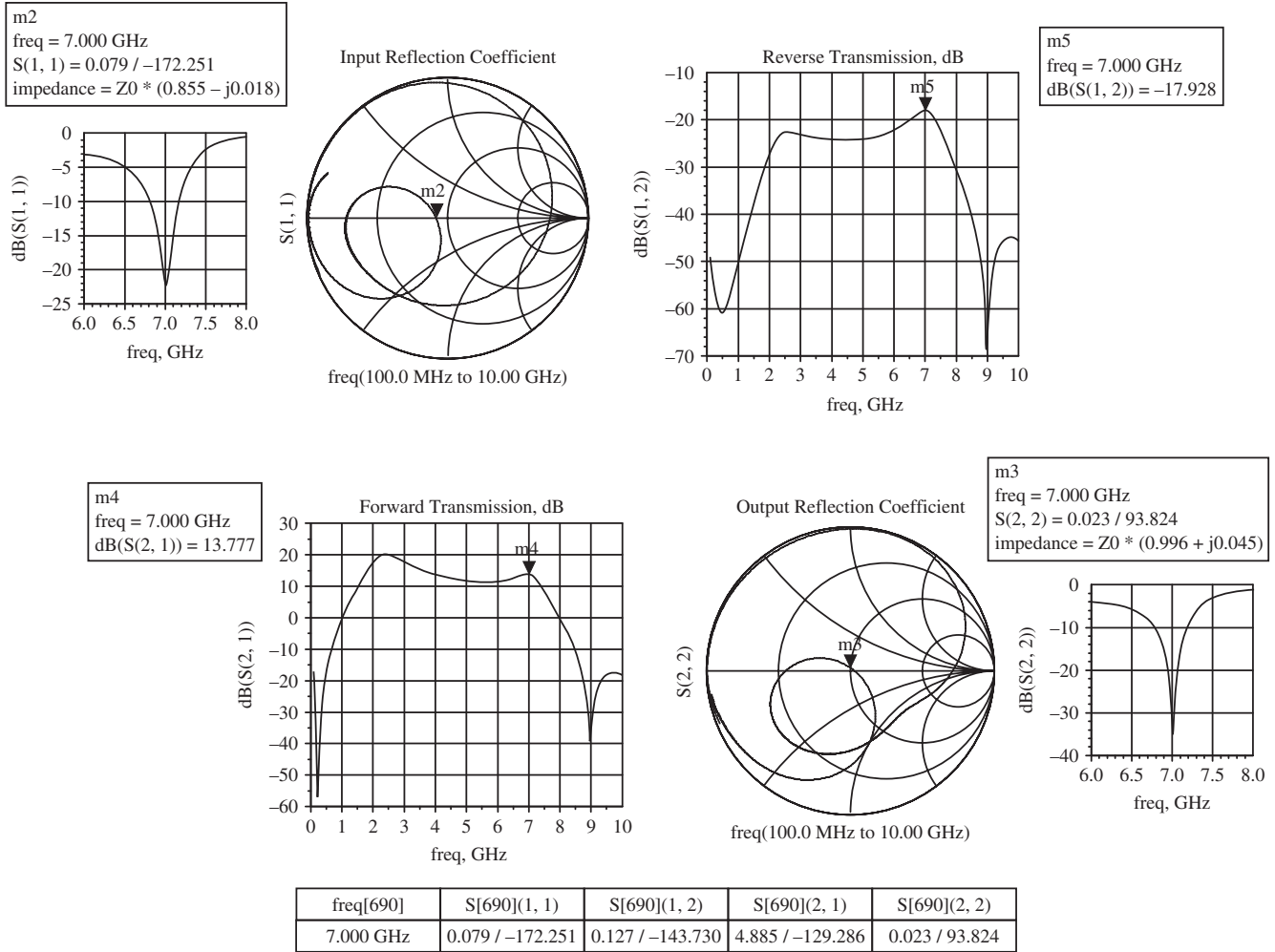


Figure 8-42 Simulated S-parameters of 7 GHz amplifier.